Cell Reports

Resource

A microscopy-based screen identifies cellular kinases modulating mitochondrial translation

Graphical abstract

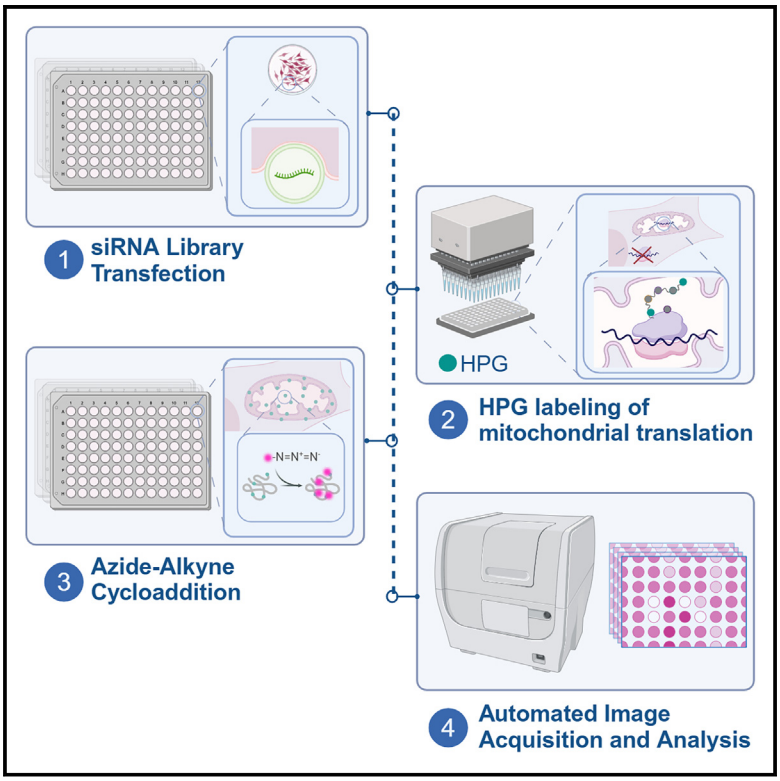

Highlights

- A fluorescent labeling screen identifies kinases regulating mt-translation
- Downregulation of cellular kinases affects mt-translation
- Several kinases are linked to mitochondrial gene expression and function
- We propose that FN3K is involved in the assembly of the mt-ribosome

Authors

Roya Yousefi, Luis Daniel Cruz-Zaragoza, Anusha Valpadashi, ..., Henning Urlaub, Peter Rehling, David Pacheu-Grau

Correspondence

luisdaniel.cruzzaragoza@med.uni-goettingen.de (L.D.C.-Z.), peter.rehling@medizin.uni-goettingen.de (P.R.)

In brief

Mitochondrial DNA encodes 13 OXPHOS subunits, which are synthesized inside the organelle. To address how mitochondrial gene expression integrates into cellular physiology, Yousefi et al. established a fluorescence-based high-throughput screen for mitochondrial translation, combining fluorescent labeling of mitochondrial translation products with siRNA-mediated knockdown. This work identifies kinases affecting mitochondrial translation.

Yousefi et al., 2025, Cell Reports *44*, 115143
January 28, 2025
https://doi.org/10.1016/j.celrep.2024.115143

CellPress

Cell Reports

CellPress
OPEN ACCESS

Resource

A microscopy-based screen identifies cellular kinases modulating mitochondrial translation

Roya Yousefi,[1,11] Luis Daniel Cruz-Zaragoza,[1,11,*] Anusha Valpadashi,[1] Carina Hansohn,[2,5] Drishan Dahal,[1] Ricarda Richter-Dennerlein,[1,3] Silvio Rizzoli,[3,4] Henning Urlaub,[2,3,5] Peter Rehling,[1,3,6,7,12,*] and David Pacheu-Grau[1,8,9,10]

[1]Department of Cellular Biochemistry, University Medical Center Göttingen, 37073 Göttingen, Germany
[2]Bioanalytical Mass Spectrometry Group, Max Planck Institute for Multidisciplinary Sciences, 37077 Göttingen, Germany
[3]Cluster of Excellence 'Multiscale Bioimaging: from Molecular Machines to Networks of Excitable Cells' (MBExC), University of Göttingen, 37075 Göttingen, Germany
[4]Department of Neuro- and Sensory Physiology, University Medical Center Göttingen, 37073 Göttingen, Germany
[5]Institute for Clinical Chemistry, University Medical Center Göttingen, 37073 Göttingen, Germany
[6]Max Planck Institute for Multidisciplinary Science, 37077 Göttingen, Germany
[7]Fraunhofer Institute for Translational Medicine and Pharmacology ITMP, Translational Neuroinflammation and Automated Microscopy, 37073 Göttingen, Germany
[8]Departamento de Bioquímica, Biología Molecular y Celular, Universidad de Zaragoza, 50009/50013 Zaragoza, Spain
[9]Instituto de Investigación Sanitaria (IIS) de Aragón, 50009 Zaragoza, Spain
[10]Centro de Investigaciones Biomédicas en Red de Enfermedades Raras (CIBERER), 28029 Madrid, Spain
[11]These authors contributed equally
[12]Lead contact
*Correspondence: luisdaniel.cruzzaragoza@med.uni-goettingen.de (L.D.C.-Z.), peter.rehling@medizin.uni-goettingen.de (P.R.)
https://doi.org/10.1016/j.celrep.2024.115143

SUMMARY

Mitochondrial DNA encodes 13 subunits of the oxidative phosphorylation (OXPHOS) system, which are synthesized inside the organelle and essential for cellular energy supply. How mitochondrial gene expression is regulated and integrated into cellular physiology is little understood. Here, we perform a high-throughput screen combining fluorescent labeling of mitochondrial translation products with small interfering RNA (siRNA)-mediated knockdown to identify cellular kinases regulating translation. As proof of principle, the screen identifies known kinases that affect mitochondrial translation, and it also reveals several kinases not yet linked to this process. Among the latter, we focus on the primarily cytosolic kinase, fructosamine 3 kinase (FN3K), which localizes partially to the mitochondria to support translation. FN3K interacts with the mitochondrial ribosome and modulates its assembly, thereby affecting translation. Overall, our work provides a reliable approach to identify protein functions for mitochondrial gene expression in a high-throughput manner.

INTRODUCTION

Mitochondria have retained their own genome during evolution. The human mitochondrial DNA (mtDNA) represents a small circular molecule that contains 37 genes. This genome encodes 13 subunits of the oxidative phosphorylation system (OXPHOS), required for the production of the bulk of cellular energy in the form of ATP, 22 tRNAs, and 2 rRNAs, required for the translation of the mtDNA-encoded OXPHOS polypeptides.[1–5] However, the vast majority of the subunits of the OXPHOS complexes are of nuclear genetic origin and must be transported into the mitochondria, where they assemble in the inner mitochondrial membrane together with mtDNA-encoded polypeptides in a precise, stoichiometric manner. This process is assisted by different assembly factors that act in stabilizing intermediate states of the assembly process or in cofactor insertion.[6–13] Interestingly, mitochondrial translation not only maintains the balance between the synthesis of mtDNA-encoded proteins and the availability of imported subunits, but it is also integrated in the cellular context. Indeed, mitochondrial protein synthesis can be modulated by different cellular stimuli.[14] For example, cellular stress response pathways such as the integrated stress response or the mitochondrial unfolded protein response have been shown to decrease mitochondrial protein synthesis.[15–17] However, a broad picture of the cellular mechanisms that influence and regulate mitochondrial translation is still missing.

Reversible phosphorylation is one of the most important mechanisms regulating protein interaction and activity in cellular processes such as metabolism, cell signaling, or cell cycle progression.[18–24] Interestingly, many different proteins inside mitochondria have been found to be phosphorylated in different model organisms or cell types.[25–31] Similar to cytosolic processes, these modifications have been reported to be involved in the regulation of critical mitochondrial processes, such as protein translocation,[32,33] fission and fusion,[34–36] mitophagy,[37–39] OXPHOS biogenesis, or mitochondrial gene expression.[40–44]

However, using MitoCarta as a reference, it was found that although 91% of mitochondrial proteins have at least one experimentally determined phosphorylation site, only 4.5% of known mitochondrial phosphosites have a functional annotation.[45] Therefore, despite the increasing evidence suggesting reversible phosphorylation as a key mechanism for the regulation of mitochondrial functions[46–48] and that kinases localize permanently or transiently to mitochondria,[49–53] the mechanistic interplay between reversible phosphorylation and mitochondrial gene expression is still missing.

Here, we present a microscopic high-throughput screening strategy based on the labeling of mitochondrial translation products using a clickable non-canonical amino acid that could be modified with fluorophores for visualization. To identify kinases that affect mitochondrial gene expression, we combined this translation product labeling strategy with a small interfering RNA (siRNA) library targeting 709 cellular protein kinases. To this end, we defined candidate kinases that down- or upregulated mitochondrial gene expression and identified not only known kinases that modulate mitochondrial translation but also unknown regulatory factors. Among these candidates, we identified fructosamine 3 kinase (FN3K), a kinase suggested to participate in glycan removal from cytosolic proteins. Our analyses show that a fraction of FN3K localizes to mitochondria and interacts with the mitochondrial ribosome. In mitochondria, FN3K affects the assembly of the ribosome and ultimately mitochondrial protein synthesis. Accordingly, a fluorescent non-canonical amino acid tagging strategy streamlined for mitochondrial translation products can be utilized to identify factors involved in mitochondrial gene expression.

RESULTS

Optical screening strategy to identify kinases affecting mitochondrial translation

We previously utilized L-homopropargylglycine (HPG), a non-canonical amino acid, for specific incorporation into mtDNA-encoded polypeptides under conditions of blocked cytosolic translation using the antibiotic harringtonine. Subsequently, we applied a copper-catalyzed cycloaddition reaction (click) to azide-containing fluorescent dyes to visualize the newly synthesized mitochondrial polypeptide chains. This strategy allowed to monitor mitochondrial translation in the context of individual cells and to obtain quantitative information about the mitochondrial protein synthesis process.[54,55] We reasoned that this approach could in principle be adapted to enable genome-wide microscopic screens to identify genes that affect mitochondrial gene expression in cells. Therefore, we established a microscopic screening approach. HeLa cells were transfected with the Silencer Human Kinase siRNA Library (Ambion) in 96-well plates. 72 h post transfection, newly synthesized mtDNA-encoded proteins were specifically labeled using HPG and subsequently coupled to the Alexa Fluor 647 azide fluorophore. Plates were imaged with an automated fluorescence microscope (Figure 1A). Intensity of mitochondrial translation measured by incorporation of HPG was assessed by quantification of the fluorescent signal. We observed only a small variation between cells present in different wells when we quantified HPG incorporation in HeLa cells (Figure S1A). To address specificity and background in the plate format, we assessed HPG incorporation for mitochondrial protein synthesis by treating cells with chloramphenicol, an inhibitor for mitochondrial translation. As expected, the signal was localized exclusively to mitochondria and was sensitive to chloramphenicol treatment (Figures 1B and 1C). Previous studies working on the quality control of mitochondrial translation showed that mitochondrial protein synthesis is affected by depletion of the inner membrane potential.[56] Therefore, in addition to chloramphenicol treatment, we analyzed HPG incorporation after incubation with the protonophore carbonyl cyanide-*m*-chlorophenylhydrazone (CCCP), to further validate the ability of our approach to address changes in mitochondrial translation upon cellular distress. As expected, HPG incorporation responded in a dose-dependent manner to CCCP titration (Figures S1B and S1C). To determine if our screening approach was suitable for detecting changes in HPG incorporation after 72 h downregulation of mitochondrial translation-related genes, we used an siRNA to downregulate DHX30 (DExH-box helicase 30), a mitochondrial ATP-dependent RNA helicase, required for proper levels of mitochondrial translation.[57,58] In agreement with the reported function of DHX30, we found a significant decrease in HPG incorporation upon silencing (Figures 1D and 1E). This reduction in mitochondrial translation was similar to that observed by [^{35}S]-methionine labeling of mitochondrial translation products in DHX30 knockdown cells (Figure S1D).

After validating the specificity and suitability of the approach, we proceeded with screening the human kinase siRNA library. We analyzed the changes in HPG incorporation after 72 h knockdown with 2,127 different siRNAs targeting all 709 known human kinase genes (using three siRNAs per gene). Cells were assayed for HPG incorporation and mitochondria stained for TOM20, and we plotted HPG incorporation versus TOM20 level for each siRNA (Figure 1F). Remarkably, mitochondrial translation did not correlate significantly with TOM20 staining (Pearson's correlation coefficient [PCC] = 0.39). Accordingly, increased or decreased HPG signals observed in cells were not due to alterations in mitochondrial amounts. Interestingly, the alteration caused by 25% of siRNAs (540 siRNAs that represent 273 kinases) modulated the HPG incorporation by more than 25% when compared to control cells. Indeed, 13% of the used siRNAs increased overall mitochondrial translation whereas 12% decreased general protein synthesis in the organelle. One putative kinase identified in the screen to decrease HPG incorporation upon knockdown was aurora kinase A interacting protein 1 (AURKAIP1) (Figure 1G). We confirmed that both mRNA and protein levels were reduced after siRNA-mediated knockdown, whereas the mRNA levels of other mitochondrial ribosome subunits were not affected (Figures 1H and 1I). In agreement with this observation, AURKAIP1, also known as mS38, was previously identified as a component of the mitochondrial ribosome (see below).[59]

In summary, selective HPG incorporation enables microscopic screening of mitochondrial translation phenotypes in the context of systematic siRNA-mediated knockdowns. The use of an siRNA library targeting cellular kinases provides a comprehensive view of potential regulatory networks to modulate mitochondrial translation.

CellPress
OPEN ACCESS

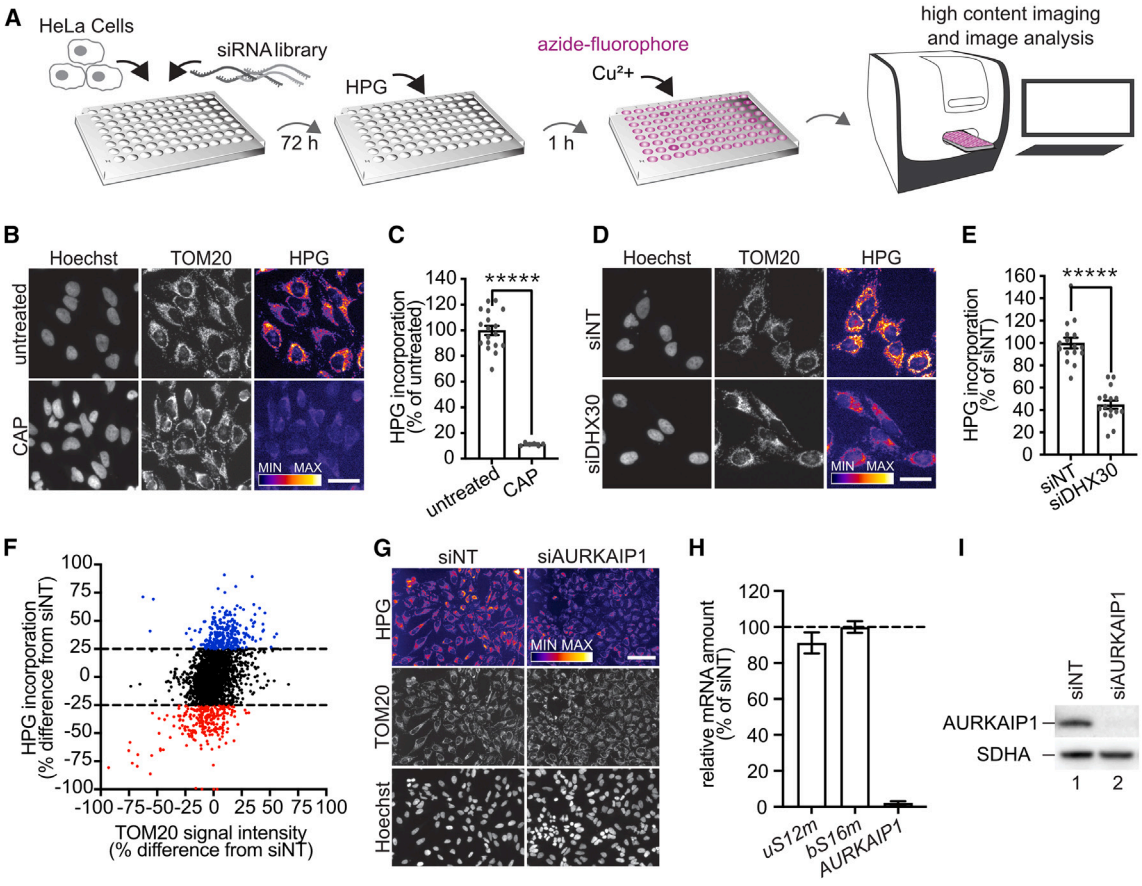

Figure 1. A screen to identify kinases linked to mitochondrial translation

(A) Schematic presentation of the screening approach.

(B) Mitochondrial translation in control and chloramphenicol (CAP)-treated cells. HPG incorporation shown in the fire lookup presentation. Hoechst, nuclei; TOM20, mitochondria. Bar, 40 μm.

(C) Quantitative analysis of HPG incorporation in CAP-treated and control cells. For each replicate, approx. 2,000 cells were analyzed in 20 images (SEM. Student's t test, $p < 0.00001$).

(D) As in (B), cells transfected with siDHX30 or non-targeting siRNA (siNT). Bar, 40 μm.

(E) As in (C), using cells transfected with siNT and siDHX30. For each replicate, approx. 2,000 cells were analyzed in 20 images (SEM. Student's t test, $p < 0.00001$).

(F) HPG incorporation plotted against TOM20 for all siRNAs transfected and labeled as in (A).

(G) siNT and siAURKAIP1-transfected cells subjected to HPG labeling as in (B). Bar, 100 μm.

(H) qPCR analysis of mRNA levels as indicated after siRNA-mediated knockdown. Samples were normalized to RPL28 (SEM, $n = 3$).

(I) Western blotting analysis of the cells transfected with either siAURKAIP1 or siNT. See also Figure S1.

Cellular kinases affect mitochondrial function and ATP levels

In order to further assess candidate kinases, we focused on genes for which more than two of the tested siRNAs changed mitochondrial protein synthesis at least 20% (either increase or decrease) in the first screen. A total of 225 siRNAs were selected and tested again for their effect on overall mitochondrial translation in three biological replicates (Figure 2A; Table S1). Nearly 50% of the tested siRNAs displayed a significant change in HPG incorporation compared to the non-targeting control (p value < 0.05) (Table S1). Interestingly, TOM20 level remained unchanged under most knockdown conditions (Figure 2A) and showed little correlation with HPG incorporation signal (PCC = 0.29, Figure S2A), again suggesting that the observed changes in mitochondrial translation were not due to mitochondrial mass differences. However, in some cases, an extremely low TOM20 level was associated with a drastic decrease in HPG incorporation. For example, polo-like kinase 1 (PLK1) knockdown decreased both HPG and TOM20 signals indicative of a broad loss in mitochondrial functionality (Figure 2A). PLK1 and other kinases that displayed a similar decrease in both TOM20 and HPG were excluded from further analysis. To this end, we focused on candidates that displayed significant effects on mitochondrial translation. By applying this filter, 84 siRNAs targeting 63 cellular kinases (46 showing decreased and 17 showing increased HPG incorporation) were selected for further investigation.

To dissect the roles of the potential modulators of mitochondrial protein synthesis, we first addressed the localization of

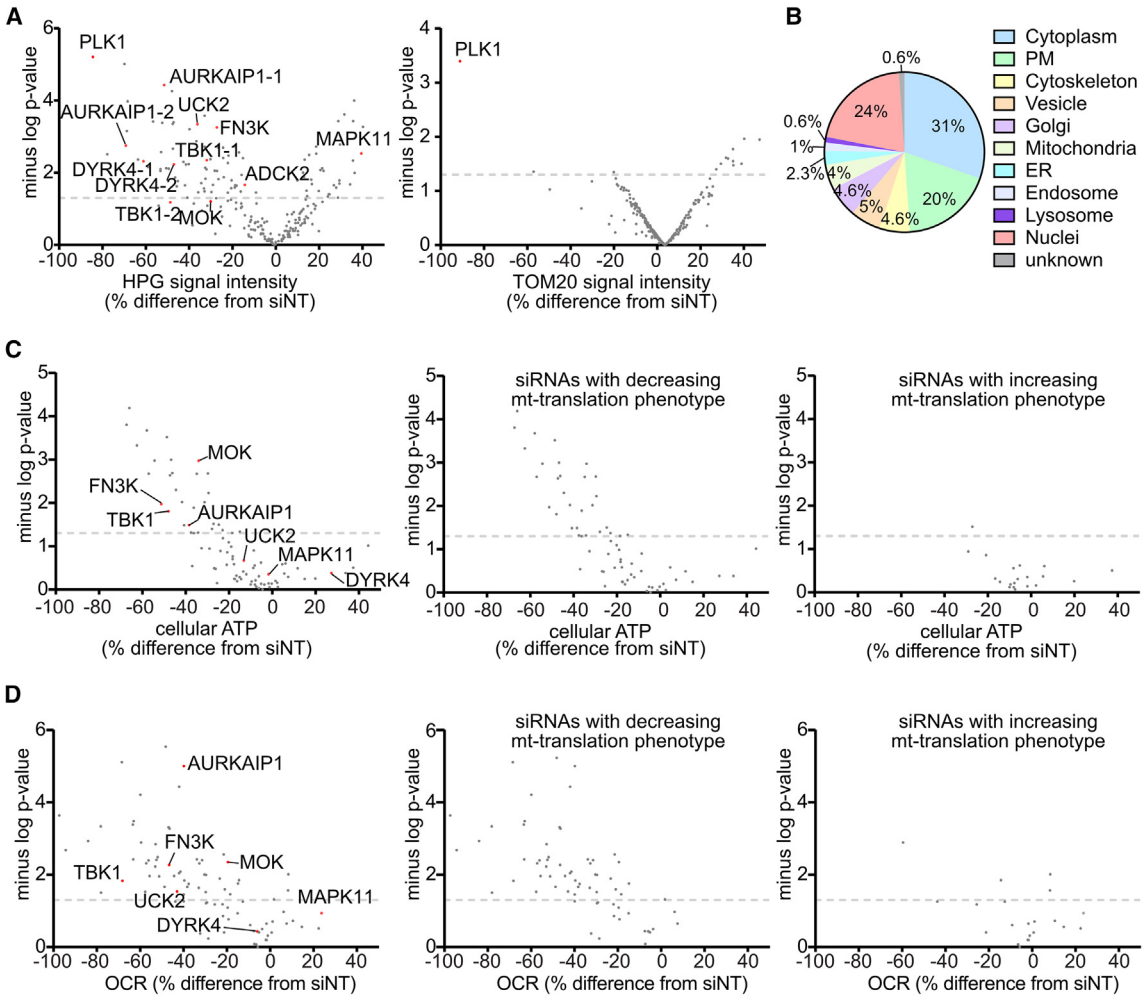

Figure 2. Cellular kinases affect mitochondrial function and ATP levels

(A) HPG incorporation and TOM20 signal after knockdown with 225 selected siRNAs (dashed line $p = 0.05$, Student's t test). Candidates of interest are presented as labeled points.

(B) Subcellular localization of kinases affecting mitochondrial translation (see Table S2).

(C) Cellular ATP levels after kinase downregulation, presenting all candidates—those with increasing or decreasing mitochondrial translation (SEM, $n = 3$, dashed line $p = 0.05$, Student's t test). Candidates of interest are presented as labeled points.

(D) Basal oxygen consumption rate (OCR) after kinase downregulation presented as in (C) (SEM, $n = 3$, dashed line $p = 0.05$, Student's t test). Candidates of interest are presented as labeled points. See also Figure S2.

these proteins in the cell. Subcellular localization information was obtained from available data from UniProt, the Human Protein Atlas,[60] MitoCarta 3.0,[61] and the Kinome Atlas.[62] While most kinases were assigned to cytosolic, nuclear, and plasma membrane localizations, interestingly, nine of the identified kinase candidates were assigned to mitochondria or had been described to be associated with mitochondria, in at least one database (Figure 2B; Table S2). Indeed, some of them were metabolic enzymes with well-described functions such as hexokinase 1, glucokinase, and mitochondrial creatine kinase 2. Another candidate found to be associated to the outer mitochondrial membrane was FKBP12-rapamycin complex-associated protein 1 (FRAP1 or mTOR). This factor regulates the expression of various nuclear-encoded mitochondrial proteins, mitochondrial function, and ATP production.[63,64] Interestingly, downregulation of any of these factors resulted in a decreased mitochondrial translation.

Mitochondrial translation products are core components of the OXPHOS system and central to the production of mitochondrial ATP. To study functional OXPHOS deficiencies derived from reduced translation of mtDNA-encoded products, we measured levels of cellular ATP and the oxygen consumption rate (OCR) after downregulation of selected kinases. Cellular ATP levels were significantly decreased upon knockdown of approximately 30% of the candidates (Figure 2C) and showed a moderate correlation between ATP content and mitochondrial translation (Figure S2B). We did not observe increased cellular ATP levels in knockdowns with an increased mitochondrial

protein synthesis. A large number of candidates (approximately 60%) displayed significantly decreased OCR, whereas only two of them showed slightly increased oxygen consumption. Accordingly, we observed a moderate to high correlation between mitochondrial translation and OCR, higher than the one observed with cellular ATP levels (Figures 2D and S2C). To summarize, we selected 84 candidate siRNAs targeting 63 cellular kinases and analyzed their effects on mitochondrial translation. Interestingly, we could observe changes in OXPHOS function upon candidate downregulation, where cellular ATP levels and OCR correlated to a certain extent with the mitochondrial protein synthesis rate observed after silencing of cellular kinases.

Cellular kinases affect energetic balance and protein synthesis

In order to further characterize some of the identified candidates and gain insights into the mechanisms driving the effect on mitochondrial translation, we selected eight kinases from the group of 63 candidates that displayed a significant effect on mitochondrial protein synthesis upon knockdown in the screen and that likely exerted their effect modulating mitochondria directly and not by an indirect metabolic effect: the AarF domain-containing kinase 2 (ADCK2), dual specificity tyrosine phosphorylation regulated kinase 4 (DYRK4), uridine-cytidine kinase 2 (UCK2), TANK-binding kinase 1 (TBK1), AURKAIP1, FN3K, MOK protein kinase (MOK), and mitogen-activated protein kinase 11 (MAPK11, also known as p38). With the exception of MAPK11, downregulation of any of the other seven candidate kinases resulted in decreased HPG incorporation when retested (Figure S3A). To define the knockdown efficiency of the tested siRNAs, we analyzed the protein levels of the target kinases after siRNA treatment and observed a clear reduction after siRNA-mediated downregulation (Figures 1I and S3B). Next, we investigated the energetic impact of the mitochondrial protein synthesis alterations upon knockdown of selected candidates and analyzed the ATP levels and OCR individually (Figure S3C). Interestingly, the extent to which ATP levels and OCR were altered in the knockdowns varied significantly. In some cases (ADCK2 and DYRK4), ATP levels and OCR were similar to the non-targeting control. In other cases (UCK2, TBK1, AURKAIP1, and FN3K), ATP levels and/or OCR were reduced compared to the controls. Interestingly, downregulation of MAPK11, which resulted in an increased mitochondrial translation, also produced a slight increase in ATP levels and OCR (Figures 3A and S3C).

Mitochondrial dysfunction may result in the inability to produce enough ATP by OXPHOS and has been described to increase glycolytic ATP production, resulting in lactic acidosis in either mitochondrial disease patients or models for neurodegenerative disorders.[65,66] Therefore, to address how the changes in cellular ATP levels, observed upon kinase downregulation, reflect changes in glycolysis or OXPHOS, we performed a time-resolved ATP synthesis assay that can independently quantify glycolytic and OXPHOS production rates. Consistent with measured cellular ATP levels and OCR, downregulation of ADCK2 had no effect on ATP synthesis rates (Figures 3A and 3B). Interestingly, glycolytic ATP production compensated a decreased OXPHOS-dependent ATP generation when DYRK4 was downregulated. In addition, both glycolytic and mitochondrial ATP productions were decreased in UCK2 and TBK1 siRNA-treated cells. Interestingly, downregulation of AURKAIP1 or FNK3K displayed a specific OXPHOS ATP production defect with no alteration of the glycolytic one. Surprisingly, we could not reproduce the significant reduction observed in cellular ATP levels and OCR in MOK siRNA-treated cells, when measuring ATP synthesis rate. In the same way, glycolytic and OXPHOS ATP production were slightly reduced in MAPK11 downregulated cells, whereas cellular ATP levels and OCR were similar to the non-targeting control (Figure 3B). In summary, our data showed that the impact of mitochondrial protein synthesis on energy metabolism was dependent on the depleted kinase. In general, diminished oxygen consumption (OCR) and total ATP levels were associated with reduced OXPHOS and ATP production or both mitochondrial and glycolytic effects. Interestingly, DYRK4 downregulation was an exception, since a significant increase of glycolytic ATP could compensate for the OXPHOS/ATP deficit.

By screening knockdown cells by HPG labeling, we were able to identify differences in bulk mitochondrial translation. Yet, this approach does not provide information about the synthesis of individual mitochondrial-encoded polypeptide chains. To close this gap in our analysis, we labeled mitochondrial translation products with [^{35}S]-methionine after knockdown of the selected kinases. Consistent with our previous results, [^{35}S]-methionine labeling after downregulation resulted in a general decreased signal compared to non-targeting control in all cases, with the exception of MAPK11, where we could observe an increased mitochondrial protein synthesis after knockdown (Figures 3C and 3D). In addition, when we quantified the radioactive signal corresponding to each individual mtDNA-encoded protein, we found that the observed changes were rather general and not due to effects on a single, specific polypeptide. However, in some cases, specific mtDNA-encoded proteins were more affected than others (Figures 3C and 3E). For example, ND2, COX1, and CYTB were most prominently affected after TBK1 knockdown. Downregulation of DYRK4, UCK2, FN3K, and MOK mostly affected the synthesis of ND3 and ND6. In AURKAIP1 downregulated cells, we could observe a general decrease in the synthesis of mtDNA-encoded polypeptides. ATP6 and ATP8 were the least affected ones. Interestingly, AURKAIP1 represents the mitoribosome-specific mtSSU protein mS38 and does not represent an active kinase.[67,68] Functional studies in yeast showed that mS38 might affect the transit of specific mRNAs and participate in the selection of mRNAs that will be translated. Indeed, the absence of yeast mS38 caused a global mitochondrial protein synthesis attenuation and prevented efficient initiation of *COX1*, *COX2*, and *COX3* mRNA translation.[69] Similarly, our analyses on AURKAIP1 downregulation in HeLa cells revealed a general decrease of mitochondrial translation. Interestingly, while the C-terminal domain of mS38 is conserved in the human homolog, the N-terminal part appears different, evidencing potential functional differences within the mitochondrial ribosome.[59] Knockdown of MAPK11 generally increased the synthesis of mitochondrial-encoded polypeptides with the exception of ND3 and ND6 that show lower synthesis levels compared to the control (Figure 3E).

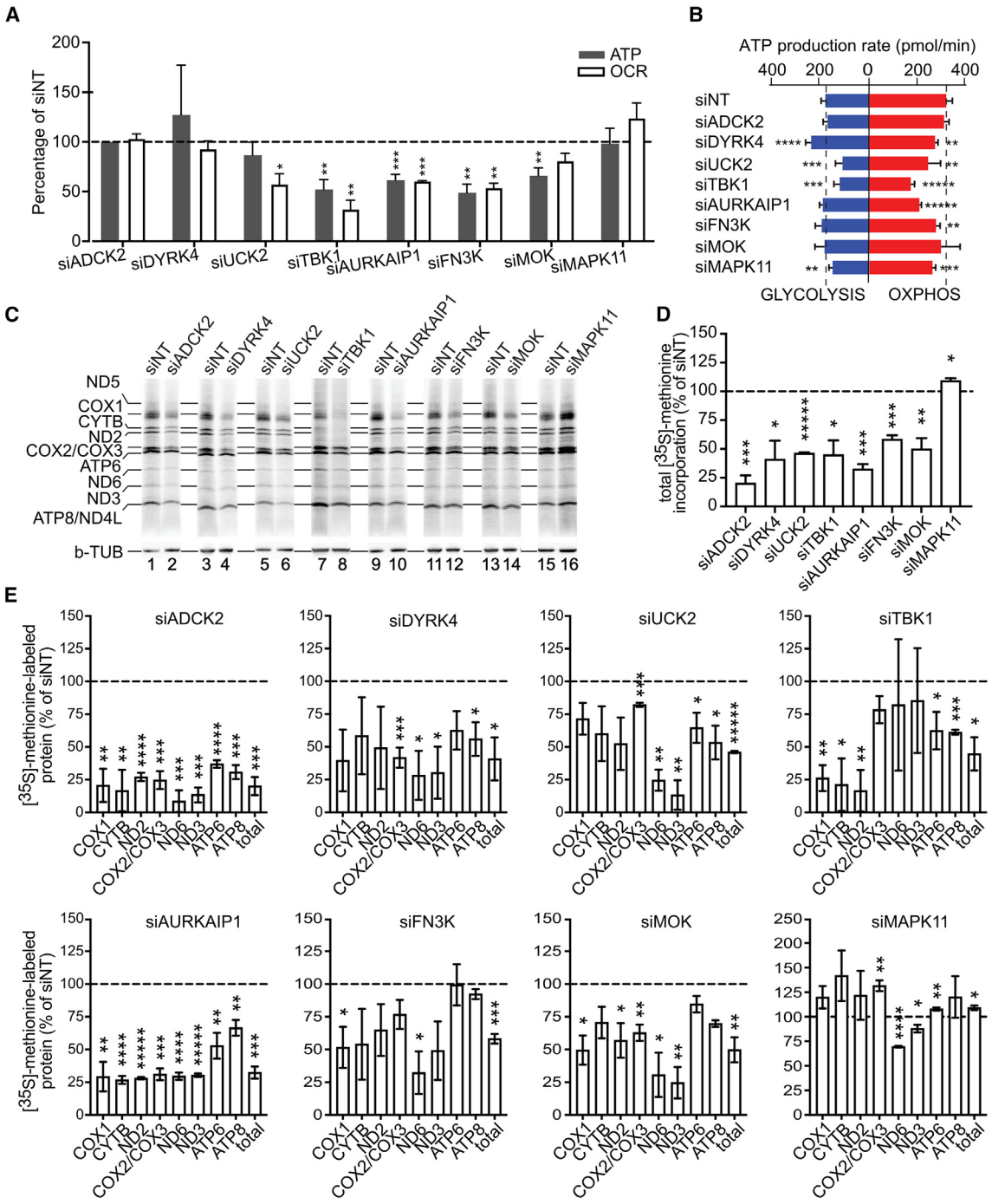

Figure 3. Cellular kinases affect energetics and protein synthesis

(A) Cellular ATP and OCR values for selected siRNAs (obtained from data in Figures 2C and 2D).

(B) Glycolysis and mitochondrial ATP rates after knockdown with selected siRNAs.

(C) [^{35}S]-methionine radiolabeling of mitochondrial translation after knockdown of selected kinases. Western blotting of b-tubulin as loading control.

(D and E) Quantification of intensity of averaged polypeptides (D) or individual ones (E) from (C) (SEM, $n = 3$).

Significance (B, D, and E) (Student's t test, $^{*}p < 0.05$, $^{**}p < 0.01$, $^{***}p < 0.001$, $^{****}p < 0.0001$, $^{*****}p < 0.00001$. See also Figure S3.

Accordingly, by silencing the expression of eight selected candidate kinases that affected mitochondrial gene expression, we revealed metabolic alterations in the affected cells. Changes of mitochondrial translation observed in our screen were confirmed by assessing the individual selected candidates with [^{35}S]-methionine labeling. Ablation of different kinases led to

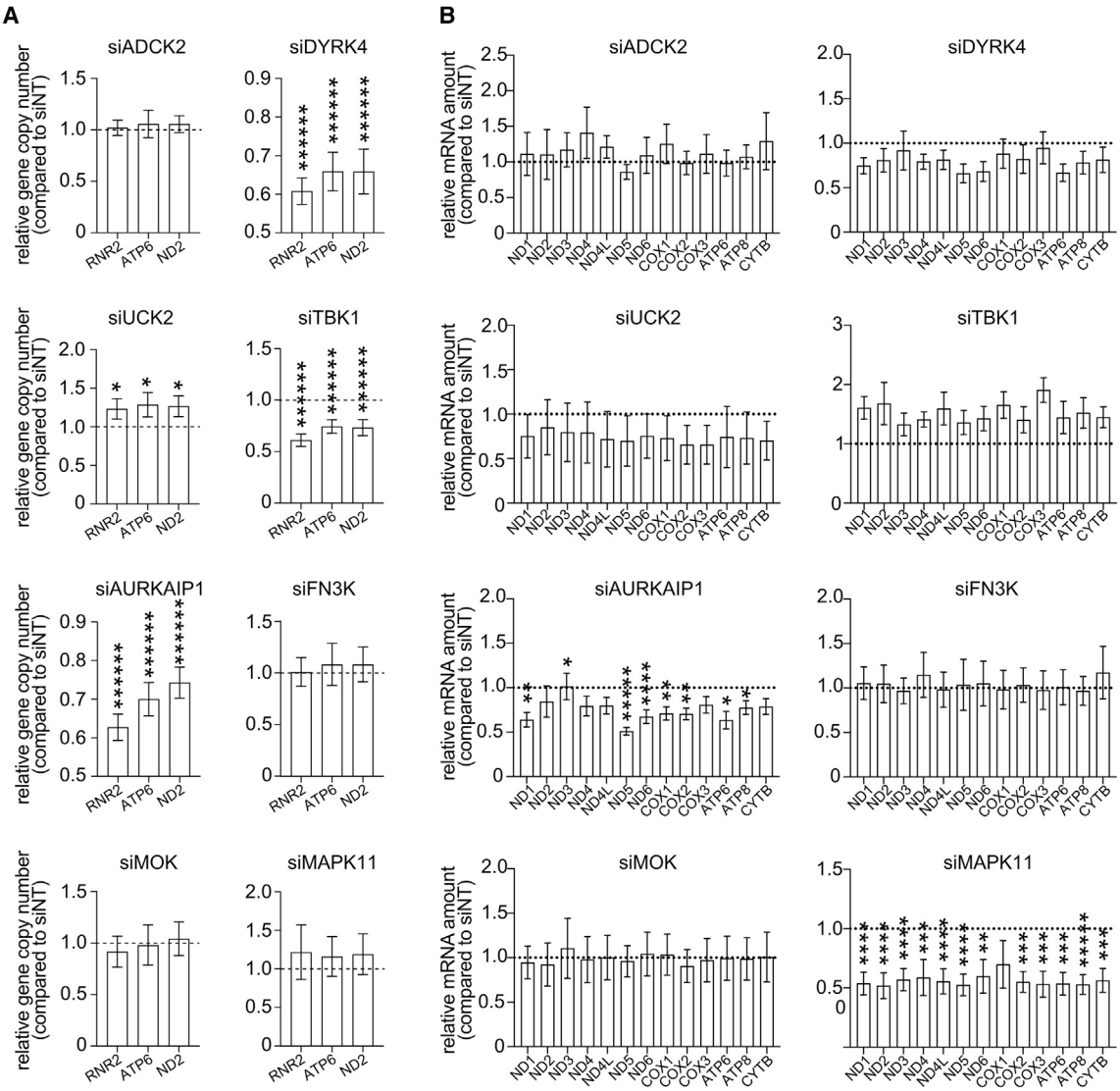

Figure 4. Kinase depletion affects mtDNA and mRNA levels

(A) mtDNA copy-number measurement after siRNA treatment (genomic primers for RNR2, ATP6, and ND2) (SEM, $n = 4$).

(B) Quantification of mitochondrial mRNA levels (real-time qPCR) after siRNA treatment (SEM, $n \geq 3$).

Significance (A and B) (Student's t test, *$p < 0.05$, **$p < 0.01$, ***$p < 0.001$, ****$p < 0.0001$, *****$p < 0.00001$, ******$p < 0.000001$).

distinct synthesis rate patterns for different mitochondrial polypeptides, and in most cases, more than one protein was affected.

mtDNA and mRNA levels upon kinase downregulation

In addition to the synthesis of mtDNA-encoded proteins, replication and transcription of mtDNA are central to the mitochondrial gene expression process. Reversible protein phosphorylation has been reported to be linked to various steps of mitochondrial gene expression. For example, DNA binding of mitochondrial transcription factor A (TFAM) is decreased by phosphorylation, and consequently, mitochondrial transcription is increased.[40,41] Phosphorylation of TFAM seems to be critical for mitochondrial localization in spermatozoids, reducing mtDNA levels and therefore explaining maternal inheritance of mtDNA.[70] In addition, mitochondrial transcription termination factor is only active when phosphorylated.[42] To address if downregulation of candidate kinases affected mtDNA or mitochondrial RNAs (mtRNAs) and consequently impact mitochondrial translation, we addressed the levels of mtDNA after siRNA treatment of selected candidates. We used three different probes directed against different genes on mtDNA (MT-RNR2, MT-ATP6, and MT-ND2). These analyses showed significantly decreased levels of mtDNA upon downregulation of DYRK4, TBK1, and AURKAIP1, whereas no differences were observed in ADCK2, FN3K, and MOK knockdown (Figure 4A). In addition, significantly increased levels of mtDNA were found after downregulation of UCK2, and a modest increase was also observed in MAPK11

downregulated cells, although it did not reach statistical significance (Figure 4A). Moreover, we analyzed the levels of mitochondrial transcripts after candidate silencing. Interestingly, the levels of mitochondrial mRNAs barely changed compared to the wild-type levels when ADCK2, DYRK4, UCK2, MOK, or FN3K were downregulated or were slightly increased in case of TBK1 knockdown. Mitochondrial transcripts were generally reduced in AURKAIP1 siRNA-treated cells (Figure 4B). Surprisingly, downregulation of MAPK11, where we had observed increased levels of mtDNA and increased mitochondrial protein synthesis, resulted in a general and significant reduction of mitochondrial mRNAs (Figure 4B). Accordingly, downregulation of kinases identified by altered mitochondrial protein synthesis could be linked to mtDNA abundance and transcription processes in some cases, whereas others need further investigation to dissect the mechanisms leading to decreased mitochondrial translation.

FN3K localizes to the mitochondrial matrix

For an in-depth analysis, we focused on the kinase FN3K. Downregulation of FN3K reduced the levels of several mtDNA-encoded polypeptides with no alteration of mtDNA or mtRNA levels (Figures 4A and 4B). FN3K has been suggested to phosphorylate fructose-ε-lysine residues in glycated proteins, destabilizing the sugar adduct and leading to the removal of glycan residue from proteins.[71–73] Interestingly, FN3K has been suggested to be present in mitochondria by immunofluorescence.[60,74] To define the localization of FN3K, we generated a C-terminally FLAG-tagged version and performed immunofluorescent microscopy experiments. We observed a colocalization of the $FN3K^{FLAG}$ with TOM20. Approximately 30% of FLAG signal per cell colocalized with mitochondria in our analysis (Figures 5A and 5B). In addition, we applied stimulated emission depletion (STED) super-resolution microscopy to define the location of FN3K within mitochondria. We detected distinct staining patterns for $FN3K^{FLAG}$ and TOM20 that resulted in different signal plot patterns when tracing straight lines in different areas of the sample. These data indicate that FN3K does not localize to the outer mitochondrial membrane (Figures 5C and 5D). In agreement, biochemical fractionation experiments showed a similar distribution of FN3K between the cytosolic and organellar fraction (Figures 5E and 5F). $FN3K^{FLAG}$ showed a similar subcellular distribution as endogenous FN3K (Figure S4A). Finally, protease protection experiments showed that $FN3K^{FLAG}$ is protected from protease treatment in purified mitochondria and mitoplasts (Figure 5G). Therefore, we concluded that a fraction of FN3K localizes to mitochondria and is present in the matrix where mitochondrial translation takes place.

Molecular determinants of FN3K mitochondrial translation regulation

The siRNA-mediated FN3K knockdown decreased the cellular growth of HeLa cells (Figure S4B). To gain further insights into the relevance of FN3K for mitochondrial and cellular function, we also analyzed the consequences of FN3K depletion in primary neurons, as an example for a more OXPHOS-dependent cellular model. FN3K knockdown in primary hippocampal cultures led to a reduction in total cell number, but surprisingly increased neurite length and astrocyte size (Figure S4C). In addition, FN3K siRNA-treated cells displayed an increased number of pre- and post-synaptic structures, but showed no changes in synaptic function (measured as the uptake, in synaptic vesicles, of an antibody directed against the vesicle protein SYT1,[75] compared to control cells; Figure S4D).

Since FN3K localized to the cytosol and nucleus, in addition to mitochondria (Figures 5A, 5B, 5E, and 5F), we address if a loss of FN3K also affected cytosolic translation and monitored HPG incorporation into cytosolic proteins in HeLa cells treated with an siRNA against FN3K. Interestingly, the incorporation of HPG into cytosolic translation products in FN3K knockdown cells was similar to the control (Figures 6A and 6B).

Since depletion of FN3K did not alter the levels of mtDNA and mtRNAs, we concluded that the mitochondrial translation defect observed after FN3K knockdown reflected an effect on the translation process or on the mitochondrial ribosome. Therefore, we assessed steady-state levels of the mitochondrial ribosome after 3 days of knockdown of FN3K. We observed similar levels of the tested large ribosomal subunit (mtLSU) constituents (mL37, mL48, mL53 uL1m) and the tested small subunit (mtSSU) constituents (uS7m, mS40, and bS16m) (Figure 6C). Taking advantage of the FLAG-tagged FN3K version, we performed immunoisolation and mass spectrometry from isolated mitochondria and analyzed FN3K-interacting partners. Interestingly, we found a significant enrichment of components of the mitochondrial ribosome and factors involved in mitochondrial translation (Figure 6D; Table S3; for complete list of proteins enriched or depleted in the immunoisolation, see also Table S3). Since the cytosolic function of FN3K was previously shown to be linked to its kinase activity, we aimed to address if the kinase activity of FN3K was required for association with the mitochondrial ribosome. Therefore, we expressed a FLAG-tagged kinase-inactive mutant version of FN3K (D210A) and performed FLAG immunoisolation. Interestingly, mutation of FN3K did not alter the subcellular distribution of the protein (Figure S4A). The FLAG immunoisolation showed that the kinase domain mutant version of FN3K displayed a significantly reduced association (up to 30%) with ribosomal small or large subunits compared to the wild-type FN3K (Figures 6E and 6F). Moreover, when we analyzed the amounts of mitochondrial mRNAs immunoisolated with the different versions of FN3K, we observed a significant reduction in co-isolation of several mRNAs isolated with mutant FN3K compared to the wild-type protein (Figure 6G). Based on these observations, we addressed if loss of FN3K affected the mitochondrial ribosome. To this end, we isolated the large ribosomal subunit using FLAG-tagged uL1m under conditions of siRNA-mediated depletion of FN3K. Surprisingly, although the amount of coimmunoprecipitated large subunit proteins was similar between control and knockdown, FN3K depletion led to lower amounts of co-isolated proteins of the small ribosomal subunit (Figure 6H). In case of mS40 and bS16m, we observed a reduction of approximately 40% compared to the control. In summary, we found that FN3K interacts with the mitochondrial ribosome. This interaction could well be relevant to the mitochondrial translation defect observed upon depletion of FN3K. Moreover, FN3K apparently affects the integrity of the mitochondrial ribosome. In addition, kinase mutant FN3K displayed decreased association to mitochondrial

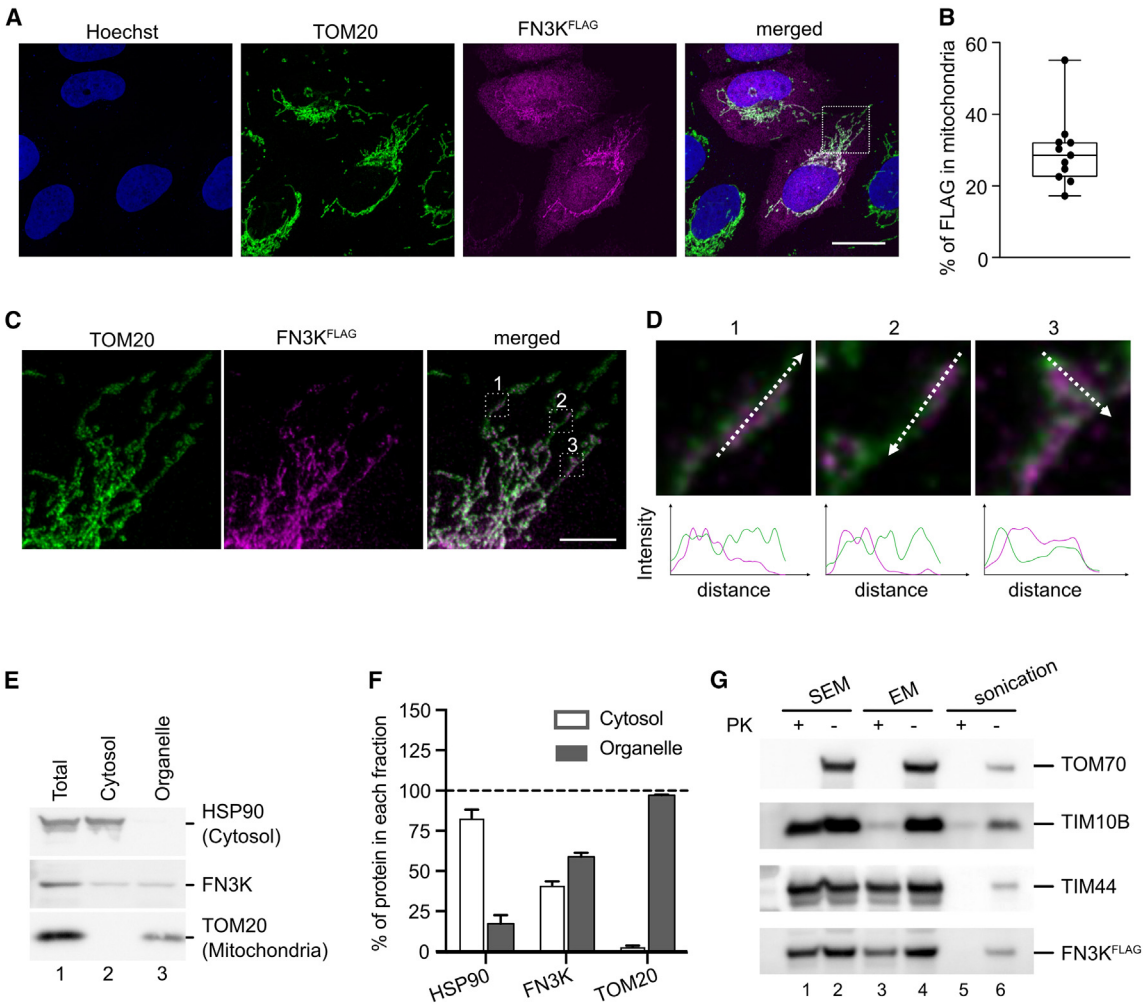

Figure 5. Mitochondrial localization of FN3K

(A) Representative confocal images of FLAG and TOM20 signals in FN3K^{FLAG}-transfected cells. Hoechst, nuclei. Bar, 20 μm.

(B) FN3K^{FLAG} signal quantification inside mitochondria (SEM, n = 11 from 2 independent experiments).

(C) Representative STED images of FLAG and TOM20 in cells as in (A). Bar, 5 μm.

(D) TOM20 and FLAG fluorescent signal profiles following depicted straight lines from selected insets in (C).

(E) Cellular fractionation experiments with wild-type HeLa cells.

(F) Quantification from (E) and similar experiments (SEM, n = 4).

(G) Western blotting analysis after protease protection assay with mitochondria isolated from FN3K^{FLAG}-expressing HeLa cells (SEM, isotonic buffer; EM, hypotonic buffer; PK, proteinase K). See also Figure S4.

mRNAs interacting with the mitochondrial ribosome. Accordingly, the kinase activity of FN3K is linked to proper mitochondrial gene expression.

DISCUSSION

In this study, we established a microscopic screen to identify regulators of mitochondrial translation using a non-canonical clickable amino acid (HPG) under conditions that enable selective incorporation into mitochondrial-encoded polypeptides. Using an siRNA library against cellular kinases, we identified 63 cellular kinases that significantly alter mitochondrial protein synthesis. The screen identified faithfully kinases with an expected impact on mitochondrial protein synthesis, such as the mitochondrial thymidine kinase TK2, the component of the mitochondrial ribosome AURKAIP1, or the central regulator of cellular metabolism mTOR.[59,63,76] 46 kinases displayed a significant decrease in HPG incorporation upon their siRNA-mediated knockdown, highlighting cellular pathways that might be relevant for mitochondrial gene expression. Several candidates identified within this group were kinases acting on metabolites rather than proteins, such as hexokinase I and hexokinase IV (glucokinase) that phosphorylate glucose. In addition, 17 kinases increased the synthesis of mtDNA-encoded proteins. Interestingly, one of the identified candidates was the MAPK-interacting protein kinase (MKNK2). Downregulation of this factor, either genetically

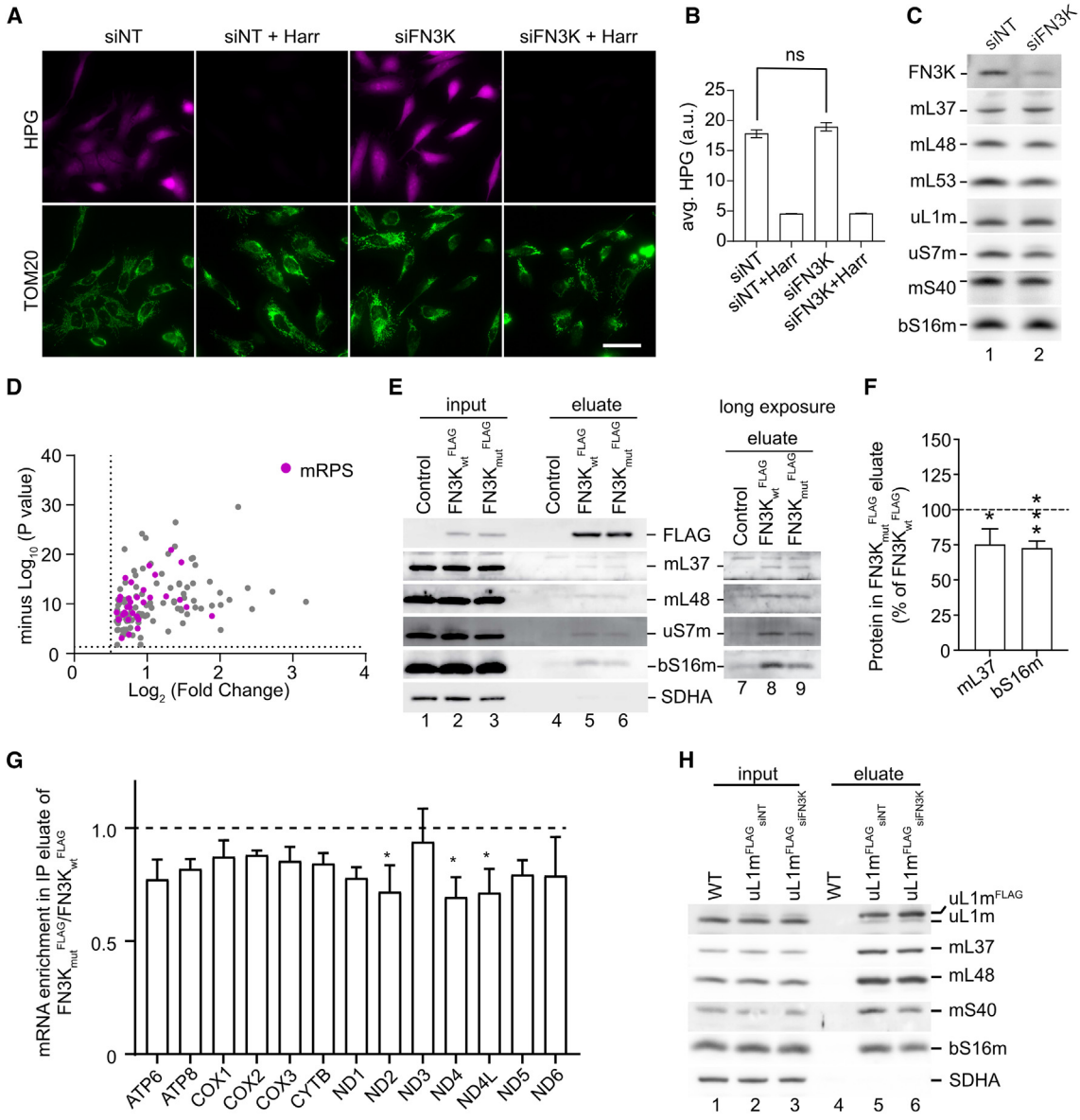

Figure 6. Molecular determinants of FN3K mitochondrial translation regulation

(A) Representative epifluorescent images of HPG in cells transfected with siNT and siFN3K in the absence or presence of harringtonine (Harr). HPG intensity in the presence of Harr has been set up to 0, and other images have been normalized by it. Bar, 50 μm.

(B) HPG quantification analysis of samples in (A) (SEM, $n \geq 100$ cells from 3 independent experiments, Student's t test).

(C) Western blotting analysis of mitoribosomal components in isolated mitochondria extracted from cells transfected as in (A).

(D) Mass spectrometry analysis after FN3K^{FLAG} immunoisolation in isolated mitochondria. Not transfected mitochondria used as control ($n = 3$ biological and technical replicates). Enriched proteins involved in mitochondrial translation (purple) and other mitochondrial proteins enriched (gray) as listed in Table S3.

(E) Western blotting analysis of mitoribosomal subunits co-isolated after wild-type or mutant (D210A) FN3K^{FLAG} immunoisolation.

(F) Quantification from (E) of the large and small mitochondrial ribosome subunits (mL37 and bS16m, respectively) co-isolated with mutant FN3K^{FLAG} compared to wild-type FN3K^{FLAG} (mean ± SEM, $n = 3$, Student's t test, $^{*}p < 0.05$, $^{***}p < 0.001$).

(G) Quantification of mitochondrial mRNA isolation after FLAG immunoprecipitation as in (E) (SEM, $n = 3$, Student's t test, $^{*}p < 0.05$).

(H) Western blotting analysis of mitoribosomal subunits after uL1m-FLAG immunoisolation of isolated mitochondria transfected as in (A). See also Figure S4.

or pharmacologically has been associated to a protection toward high-fat diet-induced obesity due to higher energy expenditure and changed expression of critical genes related to mitochondrial biogenesis, OXPHOS, or ATP consumption in murine models.[77] Further investigation would be required to dissect the mechanisms underlying improved protein synthesis of mtDNA-encoded polypeptides.

Among the identified kinases, we characterized the function of FN3K. Interestingly, FN3K was previously reported to be involved in the removal of glycan residues in the cytoplasm.[71–73] Here, we

showed that a fraction of FN3K localizes to the mitochondrial matrix. In addition, FN3K interacts with subunits of the mitochondrial ribosome and other translation factors. Reduced levels of FN3K affected the interaction between the small and large mitochondrial ribosome subunits. A reduction in fully assembled ribosomes is in agreement with the observed general decrease in mitochondrial translation, together with the decreased OXPHOS-derived ATP and oxygen consumption but with no observable changes in the levels of mtRNAs or mtDNA. In addition, we observed that kinase-inactive FN3K showed reduced interaction with the ribosome compared to the wild-type version and found a significant decrease in mitochondrial mRNA levels interacting with the ribosome in the context of mutant FN3K. Interestingly, one of the interacting partners we could identify for FN3K was mS29. This factor, also known as DAP3, has been found in the structural analysis of the mitochondrial ribosome to mediate contact between the head of the mtSSU and the central protuberance of the mtLSU.[67,78,79] In addition, phosphorylation of this protein has been shown *in vivo* and might therefore influence ribosome assembly. Although several kinases were able to phosphorylate mS29 *in vitro*,[80] to our knowledge, the identification of the responsible proteins for this activity *in vivo* is still missing, and therefore, it is tempting to speculate that FN3K might be one of the kinases phosphorylating mS29, regulating the assembly of the mitoribosome, and finally affecting mitochondrial protein synthesis.

To conclude, here, we describe an optical screen that enables identification of unknown factors that affect mitochondrial translation. In a proof-of-principle approach, we utilized siRNA-mediated knockdown of cellular kinases. Similarly, the strategy could be applied to other siRNA or knockout libraries and to different cell lines. We expect that, by monitoring translation in intact cells, a broader understanding on how mitochondrial gene expression is integrated into the cellular context can be achieved. We have identified cellular kinases that modulate mitochondrial protein synthesis and provided insights into the regulation of mitochondrial gene expression.

Limitations of the study

Mitochondrial translation is a highly energy-dependent process. Accordingly, knockdown or mutant cells that are affected in cellular energy supply will indirectly impact mitochondrial translation. Therefore, candidate regulators of translation identified in a screen require careful functional assessment. Moreover, the imaging approach shown in our study provides an assessment of bulk mitochondrial translation. Yet, it will not resolve such factors that are specific for a single translation product. Considering that different mitochondria of a given cell might display different regulation due to specific metabolic roles, super-resolution approaches would be required to assess translation phenotypes in this context.

RESOURCE AVAILABILITY

Lead contact

Further information and requests for resources should be addressed to and will be fulfilled by the lead contact, Peter Rehling (peter.rehling@medizin.uni-goettingen.de).

Materials availability

All unique/stable reagents generated in this study are available from the lead contact with a completed materials transfer agreement.

Data and code availability

- Protein interaction data on FN3K have been deposited at the Proteomics Identification Database and are publicly available as of the date of publication under accession code PXD053045 (http://www.ebi.ac.uk/pride/archive/projects/PXD053045).
- Imaging scripts used for image analysis are available upon request to the lead contact.
- Any additional information required to reanalyze the data reported in this paper is available from the lead contact upon request.

ACKNOWLEDGMENTS

We are grateful to C. Meisinger and members of the Rehling laboratory for support and discussion. This study was funded by the Deutsche Forschungsgemeinschaft under Germany's Excellence Strategy – EXC 2067/1–390729940 (P.R.), SFB1286 (projects A06/A10 [P.R. and H.U.] and A03 [S.R.]), the European Research Council (ERC) Advanced Grant MiXpress (ERCAdG no. 101095062) to P.R., DFG Emmy Noether grant (RI 2715/1-1 to R.R.-D.), and the Max Planck Society (P.R. and H.U.). D.P.-G. was supported by Agencia Estatal de Investigación (grant PID2020-116970GA-I00 and grant RYC2020-029544-I funded by MCIN/AEI/10.13039/501100011033 and by "ESF Investing in your future") and Gobierno de Aragón (Grupos Consolidados B33_23R).

AUTHOR CONTRIBUTIONS

Conceptualization, P.R., L.D.C.-Z., and D.P.-G.; methodology, R.Y., L.D.C.-Z., R.R.-D., S.R., H.U., P.R., and D.P.-G.; investigation, R.Y., L.D.C.-Z., A.V., C.H., S.R., and D.P.-G.; writing—original draft, R.Y. and D.P.-G.; writing—review and editing, R.Y., L.D.C.-Z., A.V., C.H., R.R.-D., S.R., H.U., P.R., and D.P.-G.; funding acquisition, P.R. and D.P.-G.; resources, P.R. and D.P.-G.; supervision, L.D.C.-Z., P.R., and D.P.-G.

DECLARATION OF INTERESTS

The authors declare no competing interests.

STAR★METHODS

Detailed methods are provided in the online version of this paper and include the following:

- KEY RESOURCES TABLE
- EXPERIMENTAL MODEL AND STUDY PARTICIPANT DETAILS
- METHOD DETAILS
  - Transfection of HeLa cells with human kinase siRNA library
  - HPG-labeling of mitochondrial translation in 96-well plate
  - Click-chemistry and immunostaining of fixed cells
  - Image acquisition and analysis
  - siRNA-mediated gene knockdown
  - Transient transfection of plasmid constructs
  - Real-time respirometry
  - Cellular ATP detection assay
  - Isolation of mitochondria
  - Mitochondria swelling and protease-protection assay
  - Radioactive labeling of mitochondrial translation products
  - Cellular fractionation
  - Steady-state analysis of protein level with western blotting
  - RNA extraction, cDNA synthesis and qRT-PCR
  - DNA extraction, mtDNA copy number measurement
  - FLAG immunoisolation
  - Analysis of mitochondrial RNA abundance by nanoString
  - Sample preparation for LC-MS
  - LC-MS/MS acquisition

SUPPLEMENTAL INFORMATION

Supplemental information can be found online at https://doi.org/10.1016/j.celrep.2024.115143.

Received: July 12, 2024
Revised: November 10, 2024
Accepted: December 12, 2024

REFERENCES

1. Ojala, D., Montoya, J., and Attardi, G. (1981). tRNA punctuation model of RNA processing in human mitochondria. Nature *290*, 470–474. https://doi.org/10.1038/290470a0.
2. Anderson, S., Bankier, A.T., Barrell, B.G., de Bruijn, M.H., Coulson, A.R., Drouin, J., Eperon, I.C., Nierlich, D.P., Roe, B.A., Sanger, F., et al. (1981). Sequence and organization of the human mitochondrial genome. Nature *290*, 457–465. https://doi.org/10.1038/290457a0.
3. Rackham, O., and Filipovska, A. (2022). Organization and expression of the mammalian mitochondrial genome. Nat. Rev. Genet. *23*, 606–623. https://doi.org/10.1038/s41576-022-00480-x.
4. Gustafsson, C.M., Falkenberg, M., and Larsson, N.G. (2016). Maintenance and Expression of Mammalian Mitochondrial DNA. Annu. Rev. Biochem. *85*, 133–160. https://doi.org/10.1146/annurev-biochem-060815-014402.
5. Al-Faresi, R.A.Z., Lightowlers, R.N., and Chrzanowska-Lightowlers, Z.M.A. (2019). Mammalian mitochondrial translation - revealing consequences of divergent evolution. Biochem. Soc. Trans. *47*, 1429–1436. https://doi.org/10.1042/BST20190265.
6. den Brave, F., Schulte, U., Fakler, B., Pfanner, N., and Becker, T. (2024). Mitochondrial complexome and import network. Trends Cell Biol. *34*, 578–594. https://doi.org/10.1016/j.tcb.2023.10.004.
7. Pfanner, N., Warscheid, B., and Wiedemann, N. (2019). Mitochondrial proteins: from biogenesis to functional networks. Nat. Rev. Mol. Cell Biol. *20*, 267–284. https://doi.org/10.1038/s41580-018-0092-0.
8. Dennerlein, S., Rehling, P., and Richter-Dennerlein, R. (2023). Cytochrome c oxidase biogenesis - from translation to early assembly of the core subunit COX1. FEBS Lett. *597*, 1569–1578. https://doi.org/10.1002/1873-3468.14671.
9. Brischigliaro, M., and Zeviani, M. (2021). Cytochrome c oxidase deficiency. Biochim. Biophys. Acta Bioenerg. *1862*, 148335. https://doi.org/10.1016/j.bbabio.2020.148335.
10. Protasoni, M., and Zeviani, M. (2021). Mitochondrial Structure and Bioenergetics in Normal and Disease Conditions. Int. J. Mol. Sci. *22*, 586. https://doi.org/10.3390/ijms22020586.
11. Timón-Gómez, A., Nývltová, E., Abriata, L.A., Vila, A.J., Hosler, J., and Barrientos, A. (2018). Mitochondrial cytochrome c oxidase biogenesis: Recent developments. Semin. Cell Dev. Biol. *76*, 163–178. https://doi.org/10.1016/j.semcdb.2017.08.055.
12. Timón-Gómez, A., and Barrientos, A. (2020). Mitochondrial respiratory chain composition and organization in response to changing oxygen levels. J. Life Sci. *2*. https://doi.org/10.36069/JoLS/20200601.
13. Deshwal, S., Fiedler, K.U., and Langer, T. (2020). Mitochondrial Proteases: Multifaceted Regulators of Mitochondrial Plasticity. Annu. Rev. Biochem. *89*, 501–528. https://doi.org/10.1146/annurev-biochem-062917-012739.
14. Richter-Dennerlein, R., Dennerlein, S., and Rehling, P. (2015). Integrating mitochondrial translation into the cellular context. Nat. Rev. Mol. Cell Biol. *16*, 586–592. https://doi.org/10.1038/nrm4051.
15. Mick, E., Titov, D.V., Skinner, O.S., Sharma, R., Jourdain, A.A., and Mootha, V.K. (2020). Distinct mitochondrial defects trigger the integrated stress response depending on the metabolic state of the cell. Elife *9*, e49178. https://doi.org/10.7554/eLife.49178.
16. Münch, C., and Harper, J.W. (2016). Mitochondrial unfolded protein response controls matrix pre-RNA processing and translation. Nature *534*, 710–713. https://doi.org/10.1038/nature18302.
17. Zhang, G., Wang, X., Li, C., Li, Q., An, Y.A., Luo, X., Deng, Y., Gillette, T.G., Scherer, P.E., and Wang, Z.V. (2021). Integrated Stress Response Couples Mitochondrial Protein Translation With Oxidative Stress Control. Circulation *144*, 1500–1515. https://doi.org/10.1161/CIRCULATIONAHA.120.053125.
18. Krek, W., and Nigg, E.A. (1991). Differential phosphorylation of vertebrate p34cdc2 kinase at the G1/S and G2/M transitions of the cell cycle: identification of major phosphorylation sites. EMBO J. *10*, 305–316. https://doi.org/10.1002/j.1460-2075.1991.tb07951.x.
19. Santamaría, D., Barrière, C., Cerqueira, A., Hunt, S., Tardy, C., Newton, K., Cáceres, J.F., Dubus, P., Malumbres, M., and Barbacid, M. (2007). Cdk1 is sufficient to drive the mammalian cell cycle. Nature *448*, 811–815. https://doi.org/10.1038/nature06046.
20. Gavet, O., and Pines, J. (2010). Progressive activation of CyclinB1-Cdk1 coordinates entry to mitosis. Dev. Cell *18*, 533–543. https://doi.org/10.1016/j.devcel.2010.02.013.
21. Göransson, O., Kopietz, F., and Rider, M.H. (2023). Metabolic control by AMPK in white adipose tissue. Trends Endocrinol. Metabol. *34*, 704–717. https://doi.org/10.1016/j.tem.2023.08.011.
22. Johanns, M., Hue, L., and Rider, M.H. (2023). AMPK inhibits liver gluconeogenesis: fact or fiction? Biochem. J. *480*, 105–125. https://doi.org/10.1042/BCJ20220582.
23. Lemmon, M.A., and Schlessinger, J. (2010). Cell signaling by receptor tyrosine kinases. Cell *141*, 1117–1134. https://doi.org/10.1016/j.cell.2010.06.011.
24. Rygiel, K.A., and Elkins, J.M. (2023). Recent advances in the structural biology of tyrosine kinases. Curr. Opin. Struct. Biol. *82*, 102665. https://doi.org/10.1016/j.sbi.2023.102665.
25. Reinders, J., Wagner, K., Zahedi, R.P., Stojanovski, D., Eyrich, B., van der Laan, M., Rehling, P., Sickmann, A., Pfanner, N., and Meisinger, C. (2007). Profiling phosphoproteins of yeast mitochondria reveals a role of phosphorylation in assembly of the ATP synthase. Mol. Cell. Proteomics *6*, 1896–1906. https://doi.org/10.1074/mcp.M700098-MCP200.
26. Renvoisé, M., Bonhomme, L., Davanture, M., Valot, B., Zivy, M., and Lemaire, C. (2014). Quantitative variations of the mitochondrial proteome and phosphoproteome during fermentative and respiratory growth in Saccharomyces cerevisiae. J. Proteonomics *106*, 140–150. https://doi.org/10.1016/j.jprot.2014.04.022.
27. Deng, N., Zhang, J., Zong, C., Wang, Y., Lu, H., Yang, P., Wang, W., Young, G.W., Wang, Y., Korge, P., et al. (2011). Phosphoproteome analysis reveals regulatory sites in major pathways of cardiac mitochondria. Mol. Cell. Proteomics *10*, M110.000117. https://doi.org/10.1074/mcp.M110.000117.
28. Bak, S., León, I.R., Jensen, O.N., and Højlund, K. (2013). Tissue specific phosphorylation of mitochondrial proteins isolated from rat liver, heart muscle, and skeletal muscle. J. Proteome Res. *12*, 4327–4339. https://doi.org/10.1021/pr400281r.
29. Zhao, X., León, I.R., Bak, S., Mogensen, M., Wrzesinski, K., Højlund, K., and Jensen, O.N. (2011). Phosphoproteome analysis of functional mitochondria isolated from resting human muscle reveals extensive phosphorylation of inner membrane protein complexes and enzymes. Mol. Cell. Proteomics *10*, M110. https://doi.org/10.1074/mcp.M110.000299.
30. Zhao, X., Bak, S., Pedersen, A.J.T., Jensen, O.N., and Højlund, K. (2014). Insulin increases phosphorylation of mitochondrial proteins in human skeletal muscle in vivo. J. Proteome Res. *13*, 2359–2369. https://doi.org/10.1021/pr401163t.

31. Thongboonkerd, V., and Chaiyarit, S. (2022). Gel-Based and Gel-Free Phosphoproteomics to Measure and Characterize Mitochondrial Phosphoproteins. Curr. Protoc. *2*, e390. https://doi.org/10.1002/cpz1.390.

32. Rao, S., Schmidt, O., Harbauer, A.B., Schönfisch, B., Guiard, B., Pfanner, N., and Meisinger, C. (2012). Biogenesis of the preprotein translocase of the outer mitochondrial membrane: protein kinase A phosphorylates the precursor of Tom40 and impairs its import. Mol. Biol. Cell *23*, 1618–1627. https://doi.org/10.1091/mbc.E11-11-0933.

33. Schmidt, O., Harbauer, A.B., Rao, S., Eyrich, B., Zahedi, R.P., Stojanovski, D., Schönfisch, B., Guiard, B., Sickmann, A., Pfanner, N., and Meisinger, C. (2011). Regulation of mitochondrial protein import by cytosolic kinases. Cell *144*, 227–239. https://doi.org/10.1016/j.cell.2010.12.015.

34. Tsushima, K., Bugger, H., Wende, A.R., Soto, J., Jenson, G.A., Tor, A.R., McGlauflin, R., Kenny, H.C., Zhang, Y., Souvenir, R., et al. (2018). Mitochondrial Reactive Oxygen Species in Lipotoxic Hearts Induce Post-Translational Modifications of AKAP121, DRP1, and OPA1 That Promote Mitochondrial Fission. Circ. Res. *122*, 58–73. https://doi.org/10.1161/CIRCRESAHA.117.311307.

35. Pyakurel, A., Savoia, C., Hess, D., and Scorrano, L. (2015). Extracellular regulated kinase phosphorylates mitofusin 1 to control mitochondrial morphology and apoptosis. Mol. Cell *58*, 244–254. https://doi.org/10.1016/j.molcel.2015.02.021.

36. Leboucher, G.P., Tsai, Y.C., Yang, M., Shaw, K.C., Zhou, M., Veenstra, T.D., Glickman, M.H., and Weissman, A.M. (2012). Stress-induced phosphorylation and proteasomal degradation of mitofusin 2 facilitates mitochondrial fragmentation and apoptosis. Mol. Cell *47*, 547–557. https://doi.org/10.1016/j.molcel.2012.05.041.

37. Okatsu, K., Oka, T., Iguchi, M., Imamura, K., Kosako, H., Tani, N., Kimura, M., Go, E., Koyano, F., Funayama, M., et al. (2012). PINK1 autophosphorylation upon membrane potential dissipation is essential for Parkin recruitment to damaged mitochondria. Nat. Commun. *3*, 1016. https://doi.org/10.1038/ncomms2016.

38. Callegari, S., Oeljeklaus, S., Warscheid, B., Dennerlein, S., Thumm, M., Rehling, P., and Dudek, J. (2017). Phospho-ubiquitin-PARK2 complex as a marker for mitophagy defects. Autophagy *13*, 201–211. https://doi.org/10.1080/15548627.2016.1254852.

39. Kondapalli, C., Kazlauskaite, A., Zhang, N., Woodroof, H.I., Campbell, D.G., Gourlay, R., Burchell, L., Walden, H., Macartney, T.J., Deak, M., et al. (2012). PINK1 is activated by mitochondrial membrane potential depolarization and stimulates Parkin E3 ligase activity by phosphorylating Serine 65. Open Biol. *2*, 120080. https://doi.org/10.1098/rsob.120080.

40. Wang, K.Z.Q., Zhu, J., Dagda, R.K., Uechi, G., Cherra, S.J., Gusdon, A.M., Balasubramani, M., and Chu, C.T. (2014). ERK-mediated phosphorylation of TFAM downregulates mitochondrial transcription: implications for Parkinson's disease. Mitochondrion *17*, 132–140. https://doi.org/10.1016/j.mito.2014.04.008.

41. Lu, B., Lee, J., Nie, X., Li, M., Morozov, Y.I., Venkatesh, S., Bogenhagen, D.F., Temiakov, D., and Suzuki, C.K. (2013). Phosphorylation of human TFAM in mitochondria impairs DNA binding and promotes degradation by the AAA+ Lon protease. Mol. Cell *49*, 121–132. https://doi.org/10.1016/j.molcel.2012.10.023.

42. Prieto-Martín, A., Montoya, J., and Martínez-Azorín, F. (2004). New DNA-binding activity of rat mitochondrial transcription termination factor (mTERF). J. Biochem. *136*, 825–830. https://doi.org/10.1093/jb/mvh192.

43. Ogbi, M., and Johnson, J.A. (2006). Protein kinase Cepsilon interacts with cytochrome c oxidase subunit IV and enhances cytochrome c oxidase activity in neonatal cardiac myocyte preconditioning. Biochem. J. *393*, 191–199. https://doi.org/10.1042/BJ20050757.

44. García-Bermúdez, J., Sánchez-Aragó, M., Soldevilla, B., Del Arco, A., Nuevo-Tapioles, C., and Cuezva, J.M. (2015). PKA Phosphorylates the ATPase Inhibitory Factor 1 and Inactivates Its Capacity to Bind and Inhibit the Mitochondrial H(+)-ATP Synthase. Cell Rep. *12*, 2143–2155. https://doi.org/10.1016/j.celrep.2015.08.052.

45. Niemi, N.M., and Pagliarini, D.J. (2021). The extensive and functionally uncharacterized mitochondrial phosphoproteome. J. Biol. Chem. *297*, 100880. https://doi.org/10.1016/j.jbc.2021.100880.

46. Niemi, N.M., Wilson, G.M., Overmyer, K.A., Vögtle, F.N., Myketin, L., Lohman, D.C., Schueler, K.L., Attie, A.D., Meisinger, C., Coon, J.J., and Pagliarini, D.J. (2019). Pptc7 is an essential phosphatase for promoting mammalian mitochondrial metabolism and biogenesis. Nat. Commun. *10*, 3197. https://doi.org/10.1038/s41467-019-11047-6.

47. Guo, X., Niemi, N.M., Hutchins, P.D., Condon, S.G.F., Jochem, A., Ulbrich, A., Higbee, A.J., Russell, J.D., Senes, A., Coon, J.J., and Pagliarini, D.J. (2017). Ptc7p Dephosphorylates Select Mitochondrial Proteins to Enhance Metabolic Function. Cell Rep. *18*, 307–313. https://doi.org/10.1016/j.celrep.2016.12.049.

48. Lu, W., Karuppagounder, S.S., Springer, D.A., Allen, M.D., Zheng, L., Chao, B., Zhang, Y., Dawson, V.L., Dawson, T.M., and Lenardo, M. (2014). Genetic deficiency of the mitochondrial protein PGAM5 causes a Parkinson's-like movement disorder. Nat. Commun. *5*, 4930. https://doi.org/10.1038/ncomms5930.

49. Lefkimmiatis, K., Leronni, D., and Hofer, A.M. (2013). The inner and outer compartments of mitochondria are sites of distinct cAMP/PKA signaling dynamics. J. Cell Biol. *202*, 453–462. https://doi.org/10.1083/jcb.201303159.

50. Hebert-Chatelain, E., Jose, C., Gutierrez Cortes, N., Dupuy, J.W., Rocher, C., Dachary-Prigent, J., and Letellier, T. (2012). Preservation of NADH ubiquinone-oxidoreductase activity by Src kinase-mediated phosphorylation of NDUFB10. Biochim. Biophys. Acta *1817*, 718–725. https://doi.org/10.1016/j.bbabio.2012.01.014.

51. Bertolin, G., Bulteau, A.L., Alves-Guerra, M.C., Burel, A., Lavault, M.T., Gavard, O., Le Bras, S., Gagné, J.P., Poirier, G.G., Le Borgne, R., et al. (2018). Aurora kinase A localises to mitochondria to control organelle dynamics and energy production. Elife *7*, e38111. https://doi.org/10.7554/eLife.38111.

52. Boerner, J.L., Demory, M.L., Silva, C., and Parsons, S.J. (2004). Phosphorylation of Y845 on the epidermal growth factor receptor mediates binding to the mitochondrial protein cytochrome c oxidase subunit II. Mol. Cell Biol. *24*, 7059–7071. https://doi.org/10.1128/MCB.24.16.7059-7071.2004.

53. Stefely, J.A., Reidenbach, A.G., Ulbrich, A., Oruganty, K., Floyd, B.J., Jochem, A., Saunders, J.M., Johnson, I.E., Minogue, C.E., Wrobel, R.L., et al. (2015). Mitochondrial ADCK3 employs an atypical protein kinase-like fold to enable coenzyme Q biosynthesis. Mol. Cell *57*, 83–94. https://doi.org/10.1016/j.molcel.2014.11.002.

54. Yousefi, R., Fornasiero, E.F., Cyganek, L., Montoya, J., Jakobs, S., Rizzoli, S.O., Rehling, P., and Pacheu-Grau, D. (2021). Monitoring mitochondrial translation in living cells. EMBO Rep. *22*, e51635. https://doi.org/10.15252/embr.202051635.

55. Zorkau, M., Albus, C.A., Berlinguer-Palmini, R., Chrzanowska-Lightowlers, Z.M.A., and Lightowlers, R.N. (2021). High-resolution imaging reveals compartmentalization of mitochondrial protein synthesis in cultured human cells. Proc. Natl. Acad. Sci. USA *118*, e2008778118. https://doi.org/10.1073/pnas.2008778118.

56. Richter, U., Lahtinen, T., Marttinen, P., Suomi, F., and Battersby, B.J. (2015). Quality control of mitochondrial protein synthesis is required for membrane integrity and cell fitness. J. Cell Biol. *211*, 373–389. https://doi.org/10.1083/jcb.201504062.

57. Antonicka, H., and Shoubridge, E.A. (2015). Mitochondrial RNA Granules Are Centers for Posttranscriptional RNA Processing and Ribosome Biogenesis. Cell Rep. *10*, 920–932. https://doi.org/10.1016/j.celrep.2015.01.030.

58. Cruz-Zaragoza, L.D., Dennerlein, S., Linden, A., Yousefi, R., Lavdovskaia, E., Aich, A., Falk, R.R., Gomkale, R., Schöndorf, T., Bohnsack, M.T., et al. (2021). An in vitro system to silence mitochondrial gene expression. Cell *184*, 5824–5837. https://doi.org/10.1016/j.cell.2021.09.033.

59. Koc, E.C., Cimen, H., Kumcuoglu, B., Abu, N., Akpinar, G., Haque, M.E., Spremulli, L.L., and Koc, H. (2013). Identification and characterization of

CHCHD1, AURKAIP1, and CRIF1 as new members of the mammalian mitochondrial ribosome. Front. Physiol. *4*, 183. https://doi.org/10.3389/fphys.2013.00183.

60. Thul, P.J., and Lindskog, C. (2018). The human protein atlas: A spatial map of the human proteome. Protein Sci. *27*, 233–244. https://doi.org/10.1002/pro.3307.
61. Rath, S., Sharma, R., Gupta, R., Ast, T., Chan, C., Durham, T.J., Goodman, R.P., Grabarek, Z., Haas, M.E., Hung, W.H.W., et al. (2021). MitoCarta3.0: an updated mitochondrial proteome now with sub-organelle localization and pathway annotations. Nucleic Acids Res. *49*, D1541–D1547. https://doi.org/10.1093/nar/gkaa1011.
62. Zhang, H., Cao, X., Tang, M., Zhong, G., Si, Y., Li, H., Zhu, F., Liao, Q., Li, L., Zhao, J., et al. (2021). A subcellular map of the human kinome. Elife *10*, e64943. https://doi.org/10.7554/eLife.64943.
63. Cunningham, J.T., Rodgers, J.T., Arlow, D.H., Vazquez, F., Mootha, V.K., and Puigserver, P. (2007). mTOR controls mitochondrial oxidative function through a YY1-PGC-1alpha transcriptional complex. Nature *450*, 736–740. https://doi.org/10.1038/nature06322.
64. de la Cruz López, K.G., Toledo Guzmán, M.E., Sánchez, E.O., and García Carrancá, A. (2019). mTORC1 as a Regulator of Mitochondrial Functions and a Therapeutic Target in Cancer. Front. Oncol. *9*, 1373. https://doi.org/10.3389/fonc.2019.01373.
65. Smith, A.M., Depp, C., Ryan, B.J., Johnston, G.I., Alegre-Abarrategui, J., Evetts, S., Rolinski, M., Baig, F., Ruffmann, C., Simon, A.K., et al. (2018). Mitochondrial dysfunction and increased glycolysis in prodromal and early Parkinson's blood cells. Mov. Disord. *33*, 1580–1590. https://doi.org/10.1002/mds.104.
66. Kraut, J.A., and Madias, N.E. (2010). Metabolic acidosis: pathophysiology, diagnosis and management. Nat. Rev. Nephrol. *6*, 274–285. https://doi.org/10.1038/nrneph.2010.33.
67. Amunts, A., Brown, A., Toots, J., Scheres, S.H.W., and Ramakrishnan, V. (2015). Ribosome. The structure of the human mitochondrial ribosome. Science *348*, 95–98. https://doi.org/10.1126/science.aaa1193.
68. Desai, N., Brown, A., Amunts, A., and Ramakrishnan, V. (2017). The structure of the yeast mitochondrial ribosome. Science *355*, 528–531. https://doi.org/10.1126/science.aal2415.
69. Mays, J.N., Camacho-Villasana, Y., Garcia-Villegas, R., Perez-Martinez, X., Barrientos, A., and Fontanesi, F. (2019). The mitoribosome-specific protein mS38 is preferentially required for synthesis of cytochrome c oxidase subunits. Nucleic Acids Res. *47*, 5746–5760. https://doi.org/10.1093/nar/gkz266.
70. Lee, W., Zamudio-Ochoa, A., Buchel, G., Podlesniy, P., Marti Gutierrez, N., Puigròs, M., Calderon, A., Tang, H.Y., Li, L., Mikhalchenko, A., et al. (2023). Molecular basis for maternal inheritance of human mitochondrial DNA. Nat. Genet. *55*, 1632–1639. https://doi.org/10.1038/s41588-023-01505-9.
71. Szwergold, B.S., Howell, S., and Beisswenger, P.J. (2001). Human fructosamine-3-kinase: purification, sequencing, substrate specificity, and evidence of activity in vivo. Diabetes *50*, 2139–2147. https://doi.org/10.2337/diabetes.50.9.2139.
72. Delpierre, G., Rider, M.H., Collard, F., Stroobant, V., Vanstapel, F., Santos, H., and Van Schaftingen, E. (2000). Identification, cloning, and heterologous expression of a mammalian fructosamine-3-kinase. Diabetes *49*, 1627–1634. https://doi.org/10.2337/diabetes.49.10.1627.
73. Veiga da-Cunha, M., Jacquemin, P., Delpierre, G., Godfraind, C., Théate, I., Vertommen, D., Clotman, F., Lemaigre, F., Devuyst, O., and Van Schaftingen, E. (2006). Increased protein glycation in fructosamine 3-kinase-deficient mice. Biochem. J. *399*, 257–264. https://doi.org/10.1042/BJ20060684.
74. Thul, P.J., Åkesson, L., Wiking, M., Mahdessian, D., Geladaki, A., Ait Blal, H., Alm, T., Asplund, A., Björk, L., Breckels, L.M., et al. (2017). A subcellular map of the human proteome. Science *356*, eaal3321. https://doi.org/10.1126/science.aal3321.
75. Truckenbrodt, S., Viplav, A., Jähne, S., Vogts, A., Denker, A., Wildhagen, H., Fornasiero, E.F., and Rizzoli, S.O. (2018). Newly produced synaptic vesicle proteins are preferentially used in synaptic transmission. EMBO J. *37*, e98044. https://doi.org/10.15252/embj.201798044.
76. Berardo, A., Domínguez-González, C., Engelstad, K., and Hirano, M. (2022). Advances in Thymidine Kinase 2 Deficiency: Clinical Aspects, Translational Progress, and Emerging Therapies. J. Neuromuscul. Dis. *9*, 225–235. https://doi.org/10.3233/JND-210786.
77. Sandeman, L.Y., Kang, W.X., Wang, X., Jensen, K.B., Wong, D., Bo, T., Gao, L., Zhao, J., Byrne, C.D., Page, A.J., and Proud, C.G. (2020). Disabling MNK protein kinases promotes oxidative metabolism and protects against diet-induced obesity. Mol. Metabol. *42*, 101054. https://doi.org/10.1016/j.molmet.2020.101054.
78. Greber, B.J., Bieri, P., Leibundgut, M., Leitner, A., Aebersold, R., Boehringer, D., and Ban, N. (2015). Ribosome. The complete structure of the 55S mammalian mitochondrial ribosome. Science *348*, 303–308. https://doi.org/10.1126/science.aaa3872.
79. Singh, V., Itoh, Y., Del'Olio, S., Hassan, A., Naschberger, A., Flygaard, R.K., Nobe, Y., Izumikawa, K., Aibara, S., Andréll, J., et al. (2023). Structure of mitoribosome reveals mechanism of mRNA binding, tRNA interactions with L1 stalk, roles of cofactors and rRNA modifications. bioRxiv. https://doi.org/10.1101/2023.05.24.542018.
80. Miller, J.L., Koc, H., and Koc, E.C. (2008). Identification of phosphorylation sites in mammalian mitochondrial ribosomal protein DAP3. Protein Sci. *17*, 251–260. https://doi.org/10.1110/ps.073185608.
81. Estell, C., Stamatidou, E., El-Messeiry, S., and Hamilton, A. (2017). imaging of mitochondrial translation shows weak correlation with nucleoid DNA intensity and no suppression during mitosis. J. Cell Sci. *130*, 4193–4199. https://doi.org/10.1242/jcs.206714.
82. Kaech, S., and Banker, G. (2006). Culturing hippocampal neurons. Nat. Protoc. *1*, 2406–2415. https://doi.org/10.1038/nprot.2006.356.
83. Banker, G.A., and Cowan, W.M. (1977). Rat hippocampal neurons in dispersed cell culture. Brain Res. *126*, 397–425. https://doi.org/10.1016/0006-8993(77)90594-7.
84. Pacheu-Grau, D., Wasilewski, M., Oeljeklaus, S., Gibhardt, C.S., Aich, A., Chudenkova, M., Dennerlein, S., Deckers, M., Bogeski, I., Warscheid, B., et al. (2020). COA6 Facilitates Cytochrome c Oxidase Biogenesis as Thiol-reductase for Copper Metallochaperones in Mitochondria. J. Mol. Biol. *432*, 2067–2079. https://doi.org/10.1016/j.jmb.2020.01.036.
85. Gomkale, R., Cruz-Zaragoza, L.D., Suppanz, I., Guiard, B., Montoya, J., Callegari, S., Pacheu-Grau, D., Warscheid, B., and Rehling, P. (2020). Defining the Substrate Spectrum of the TIM22 Complex Identifies Pyruvate Carrier Subunits as Unconventional Cargos. Curr. Biol. *30*, 1119–1127. https://doi.org/10.1016/j.cub.2020.01.024.
86. Mick, D.U., Dennerlein, S., Wiese, H., Reinhold, R., Pacheu-Grau, D., Lorenzi, I., Sasarman, F., Weraarpachai, W., Shoubridge, E.A., Warscheid, B., and Rehling, P. (2012). MITRAC links mitochondrial protein translocation to respiratory-chain assembly and translational regulation. Cell *151*, 1528–1541. https://doi.org/10.1016/j.cell.2012.11.053.
87. Chomyn, A. (1996). In vivo labeling and analysis of human mitochondrial translation products. Methods Enzymol. *264*, 197–211. https://doi.org/10.1016/s0076-6879(96)64020-8.

STAR★METHODS

KEY RESOURCES TABLE

REAGENT or RESOURCE	SOURCE	IDENTIFIER
Antibodies		
Anti human ATP5B	Custom made	N/A
Anti human SDHA	Thermo Fisher Scientific	Cat# 459200, RRID:AB_1083801
Anti human AURKAIP1	Thermo Fisher Scientific	Cat# PA5-56869, RRID:AB_2638401
Anti human TOM70	Thermo Fisher Scientific	Cat# PA5-83890, RRID:AB_2791042
Anti human TIM44	Custom made	N/A
Anti human TIM10B	Custom made	N/A
Anti human b-tubulin	abcam	Cat# ab6046, RRID:AB_2210370
Anti human TOM20	Proteintech	Cat# 11802-1-AP, RRID:AB_2207530
Anti human MRPL1 (mL1)	Proteintech	Cat# 16254-1-AP, RRID:AB_2145582
Anti human MRPL53 (mL53)	Proteintech	Cat# 16142-1-AP, RRID:AB_2878223
Anti human MRPS25	Proteintech	Cat# 67903-1-Ig, RRID:AB_2918659
Anti human mL37	Proteintech	Cat# 15190-1-AP, RRID:AB_2146040
Anti human mL48	Proteintech	Cat# 14677-1-AP, RRID:AB_2282151
Anti human uS7m	Proteintech	Cat# 26828-1-AP, RRID: AB_2146040
Anti human mS40	Custom made	N/A
Anti human bS16m	Proteintech	Cat# 16735-1-AP, RRID:AB_2180166
Anti human FN3K	Proteintech	Cat# 14293-1-AP, RRID:AB_2105975
Anti FLAG	Sigma-Aldrich	Cat# F1804, RRID:AB_262044
Anti human HSP90	Cell Signaling	Cat#4874S, RRID:AB_2121214
Biological samples		
Rat: Primary hippocampal neuronal cells	This study	N/A
Chemicals, peptides, and recombinant proteins		
FLAG-peptide	SIGMA	Cat# F4799
Lipofectamine® RNAiMAX	Thermo Fisher Scientific	Cat# 13778075
Harringtonine	Carbosynth	Cat# FH15975
HPG	Thermo Fisher Scientific	Cat# C10186
Hoechst 33342	Thermo Fisher Scientific	Cat# 62249
TurboFect	Life Technologies	Cat# R0533
OptiMEM	Thermo Fisher Scientific	Cat# 11058021
PEI	Polysciences Europe GmbH	Cat# 24765-100
AlexaFluor 647-azide	Thermo Fisher Scientific	Cat# A10277
TRIzol	Thermo Fisher Scientific	Cat# 15596026
Critical commercial assays		
Click-iT Cell Reaction Buffer Kit	Thermo Fisher Scientific	Cat# C10269
Luminescent ATP Detection Assay Kit	Abcam	Cat# ab113849
CyQuant cell proliferation assay	Thermo Fisher Scientific	Cat# C7026
RNA Clean&Concentrator kit	Zymo Reseach	Cat# R1091
First Strand cDNA Synthesis kit	Thermo Fisher Scientific	Cat# K1612
SensiMixTM SYBR Low-Rox Obe Step kit	Bioline	Cat# QT625-02
PureLink Genomic DNA mini kit	Thermo Fisher	Cat# K182001
TaqMan Universal PCR master mix	Applied Biosystems	Cat# 4326708
anti-FLAG M2 Affinity Gel	Sigma-Aldrich	Cat# A2220

(*Continued on next page*)

Continued

REAGENT or RESOURCE	SOURCE	IDENTIFIER
Deposited data		
Protein interaction FN3K-FLAG-MS data	PRIDE	PXD053045
Experimental models: Cell lines		
Human: HeLa cells	DSMZ collection (Leibnitz institute)	DSMZ Cat# ACC-57, RRID:CVCL_0030
Human: HEK293T Flp-In™ TREX™	Thermo Fisher Scientific	RRID:CVCL_U427
Oligonucleotides		
Silencer™ Human Kinase siRNA Library	Thermo Fischer Scientific	Cat# A30079
Taqman MT-RNR2	Applied Biosystems	Cat# 4331182
Taqman MT- AFP6	Applied Biosystems	Cat# 4331182
Taqman MT- ND2	Applied Biosystems	Cat# 4331182
Taqman 18S rRNA	Applied Biosystems	Cat# 4331182
TagSet-24	nanoString	121000602
Recombinant DNA		
FN3K (WT)-FLAG in pcDNA 3.1/	Genscript	N/A
FN3K (MUT, D210A)-FLAG in pcDNA 3.1/	Genscript	N/A
Software and algorithms		
MATLAB	The Mathworks, Inc., Natick, MA	https://www.mathworks.com/products/matlab.html
Huygens software	Scientific Volume Imaging	www.svi.nl
Agilent Seahorse analytics software	WAVE	RRID:SCR_013575 http://www.agilent.com/
FIJI	FIJI	RRID:SCR_002285
Spectronaut	Biognosys	https://biognosys.com/resources/spectronaut-a-groundbreaking-increase-in-identifications/
Other		
Automated pipetting system Biomek FXP	Beckman Coulter	RRID:SCR_008940
Cytation 5™ Cell Imaging Multi-Mode Reader BioTek	Biotek	RRID:SCR_019732
Abberior microscope with Imspector imaging software operator	Abberior Instruments	RRID:SCR_015249
XF96 Extracellular Flux Analyzer	Seahorse Bioscience	RRID:SCR_013575
Typhoon scanner	GE Healthcare	RRID:SCR_025702
QuantStudio 6 flex cycler	Applied Biosystems	–
Nanodrop	Thermo Fischer Scientific	RRID:SCR_018042
nCounter® MAX analysis system	nanoString	RRID:SCR_023912
BioRuptor device	Diagenode	–
timsTOF Pro2	Bruker	RRID:SCR_023608
Ultimate 3000 RSLCnano UHPLC system	Thermo Fisher Scientific	RRID:SCR_008452
C18 PepMap100-trapping column	Thermo Fisher Scientific	RRID:SCR_008452
Column Aurora with CSI	IonOpticks	RRID:SCR_024593

EXPERIMENTAL MODEL AND STUDY PARTICIPANT DETAILS

HeLa cells (female, RRID: CVCL_0030) were purchased from the DSMZ collection at the Leibnitz institute. HEK293T Flp-In TREX cell line (female, RRID:CVCL_U427) was purchased from Thermo Fisher. Cells were cultured in Dulbecco's modified Eagle's medium (DMEM, ThermoFischer), supplemented with 10% (V/V) fetal bovine serum (FBS, Biochrom), 1 mM sodium pyruvate, 2 mM L-glutamine, and 50 μg/mL uridine. Cells were cultured at 37°C in the incubator with 5% CO_2 and passaged regularly. For imaging purposes, cells were seeded on glass coverslips or glass-bottom Sensoplates (Greiner), coated with 0.1 mg/mL poly-L-lysine (sigma, P2658). Rat primary hippocampal neuronal cells were obtained and cultured exactly as described.[75]

METHOD DETAILS

Transfection of HeLa cells with human kinase siRNA library

Silencer Human Kinase siRNA Library was purchased from ThermoFischer (A30079). Nuclease-free water was added to the original plates to make a concentration of 2 μM. Running plates of 166 nM were prepared in 96-well PCR plates and were used for transfection. Reverse transfection was performed according to the manufacturer's protocol with slight modifications. Briefly, for each well of 96-well Sensoplate, 0.2 μL of Lipofectamine RNAiMAX (Invitrogen) was diluted in 20 μL of OptiMEM (Gibco), mixed and incubated for 5 min. From the siRNA running plate, 5 μL was added to the OptiMEM-Lipofectmaine mixture and incubated for 20 min. Meanwhile, 4000 cells per well were counted in 100 μL of media and were added to the plate after incubation. For respirometry analysis, the transfection was performed in Seahorse 96-well microplates (Agilent) with 2500 cells per well. The plates were then incubated for 72 h at 37°C in the incubator with 5% CO_2, wrapped in humid tissues to minimize evaporation.

HPG-labeling of mitochondrial translation in 96-well plate

To label mitochondrial translation in 96-well plate, we adapted a click-chemistry based method that was previously introduced by us and others.[54,55,81] Cells were incubated with methionine-free DMEM media containing 200 μM harringtonine (Carbosynth, FH15975) for 10 min. The media was changed to methionine-free DMEM containing harringtonine, plus 500 μM of L-Homopropargylglycine (HPG, ThermoFisher, C10186) and was incubated for 1 h at 37°C. Then, the media was removed and the cells were washed with an ice-cold permeabilizing buffer containing 10mM HEPES, 10mM NaCl, 5mM KCl, 300 mM sucrose, and 0.015% digitonin, for 2 min. A quick wash with the same buffer without digitonin was performed for 15 s. The buffer was removed and 4% PFA solution (pH 7.5, in PBS) was added to fix the cells for 30 min at room temperature. In negative control samples, 150 μg/mL chloramphenicol, freshly prepared in ethanol, was used 50 min before the labeling to stop mitochondrial translation. To maintain the timing and the solution volumes precise in all the wells, an automated pipetting system was used (Biomek FXP).

Click-chemistry and immunostaining of fixed cells

After PFA fixation, cells were washed for 5 min with PBS and quenched for 15 min with 100 mM NH4Cl in PBS. Cells were blocked and permeabilized with the staining solution (PBS with 5% BSA, 5% tryptone peptone and 0.1% Triton X-100) 3 cycles of 5 min each. After a brief wash with 3% BSA in PBS, cells were clicked for 40 min using Click-iT Cell Reaction Buffer Kit (ThermoFisher) containing 1.5 μM AlexaFluor 647-azide (ThermoFisher). After washing with 3% BSA in PBS, primary (TOM20 at 1:800 dilution, Proteintech, 11802-1-AP) and secondary (goat anti-rabbit Alexa Fluor Plus 488 at 1:800 dilution, ThermoFisher, A32731) antibodies were applied sequentially for 1 h each. Between antibody incubations, cells were washed with staining solution 3 cycles of 5 min. Same number of washes with blocking solution (PBS containing 5% BSA and 5% tryptone peptone), high-salt PBS (PBS supplemented with 500 mM NaCl), and normal PBS were performed after the secondary antibody, to thoroughly remove unspecific staining of the antibodies. For cells on coverslips, embedding was performed in Mowiol (Calbiochem, Billerica, MA, USA) and the coverslips were allowed to dry overnight at room temperature before imaging. For the library screening experiments, the nuclei were stained with 2 μM Hoechst 33342 (62249, Thermo Fisher) for 5 min, followed by a 5 min wash with PBS. The plates were kept at 4°C in dark and were imaged within 24 h.

Image acquisition and analysis

For the library screening, the 96-well Sensoplates were imaged using a Cytation 5 Cell Imaging Multi-Mode Reader BioTek (Winooski, VT, USA) equipped with a Sony CCD 16-bit grayscale camera. At least 20 images were acquired per well with a 20×, 0.45 NA objective. We used a custom macro written in MATLAB (The Mathworks, Inc., Natick, MA, USA) to analyze the images. The nuclei staining was used to spot the cells by applying a threshold. The selected regions of the nuclei were dilated to cover the whole cell area. HPG and TOM20 signals were measured for each cell area. The signals from all the cells were then averaged and normalized to the signal from the controls. The script is available upon request.

Confocal images of Figure 5 were captured using an Abberior microscope with Imspector imaging software operator (Abberior Instruments, Göttingen, Germany) equipped with a UPlanSApo 100×/1.4 NA oil immersion objective (Olympus Corporation, Japan). Pulsed 561-nm and 640-nm lasers were used for excitation. In STED images, an easy3D module 775nm laser was used for depletion. Due to high power of the laser used for imaging, bleaching of the signal occurs, which dampens FN3K staining in the cytosolic region. Huygens software (Scientific Volume Imaging, www.svi.nl) was used to deconvolve the images, where mentioned.

siRNA-mediated gene knockdown

siRNA targeting selected kinases and a non-targeting siRNA (siNT) were purchased from Eurogentec (Liege, Belgium). Cells were transfected with Lipofectamine RNAiMAX (Invitrogen) according to the manufacturer's protocol. The number of cells used for transfection in 6-well plates, T25 flasks, and 155mm plates were $0.4x10^6$, $1x10^6$, and $7x10^6$, respectively. The final siRNA concentration for HeLa cells was 33nM and for HEK cells was 50nM.

Forward transfection was performed on primary neuron culture 6 days after they were seeded at a density of approximately 30,000/cm^2 on coverslips coated with 1 mg/ml PLL according to the established protocols.[75,82,83] For each well, 0.8 μL of

lipofectamine was diluted in 200 μL OptiMEM, before the addition of 1.6 μL of siRNA stock of 20 μM. 20 min after, the mixture was added slowly to the cells and 5 after days, cells were used for fluorescent immunostaining.

Transient transfection of plasmid constructs

The FN3K ORF and FN3K kinase-dead mutant (D210A) in a pcDNA3.1 vector, in frame with a C-terminal FLAG tag, were purchased from Genscript (Leiden, the Netherlands).

HeLa cells were transfected using TurboFect transfection reagent (R0533, Life Technologies GmbH) according to the manufacturer's protocol. Briefly, cells were seeded 1–2 days in advance on 12-well plates containing PLL-coated glass coverslips for the immunofluorescent microscopy experiments. First, 0.5μg of plasmid was diluted in OptiMEM followed by TurboFect addition to the mixture which was incubated for 15 min at room temperature. The mixture was then uniformly added to the cells which were cultured for 24 h after transfection.

For FLAG immunoisolation experiments, the transfection was performed using PEI (polyethylenimin) transfection reagent. Briefly, cells were seeded to a 50%-confluency two days prior transfection. PEI was diluted to 2 mg/mL in OptiMEM and incubated at RT for 5min and brought up to a final volume of 5 mL. In a separate tube, 20 μg plasmid DNA was diluted in 1 mL OptiMEM, mixed with 1 mL of PEI/OptiMEM solution and incubated at RT for 20 min. Solution was finally diluted with 10 mL DMEM media and carefully added to 145 mm plates containing cells. After 1h incubation additional 10 mL DMEM were added to the cells that were cultured for 24 h after transfection.

Real-time respirometry

Real-time respirometry for oxygen consumption rate (OCR) was performed with an XF96 Extracellular Flux Analyzer (Seahorse Bioscience, Billerica, MA, USA) as previously described.[84] Briefly, cell media was changed to Seahorse assay media and was calibrated at 37°C for 1 h in an incubator without CO2. The sensors were calibrated and the cell plate was placed into the analyzer. Three different measurements of oxygen levels were measured before and after addition of different inhibitors/uncouplers (3 μM oligomycin, 1.6 μM FCCP, and 1 μM antimycin A plus 1 μM rotenone). OCR was calculated from the slope of oxygen level change over the course of time. To measure the real-time ATP production rate from mitochondrial respiration and glycolysis, similar approach was performed with a slightly different order of inhibitors: 3 μM oligomycin followed by 1 μM antimycin A plus 1 μM rotenone. Extracellular acidification rate (ECAR) and OCR measurements were used to calculate the ATP production rate using the Agilent Seahorse analytics software (WAVE).

Cellular ATP detection assay

The cellular ATP was measured using Luminescent ATP Detection Assay Kit (abcam, ab113849) according to the manufacturer's protocol. Briefly, cells were lysed using detergent and then, the substrate was added. Luminiscent signal was detected using a plate reader (Agilent BioTek). The values were normalized to the number of cells measured by parallel CyQuant cell proliferation assay (Thermo, C7026).

Isolation of mitochondria

For mitochondria swelling and protease protection assays, HeLa cells were rinsed with a cold isotonic buffer containing 10 mM MOPS at pH 7.2, 225 mM sucrose, 75 mM mannitol, and 1 mM EGTA. The weight of the cell pellet was then measured. The pellet was reconstituted (5mL per 1g of cells) in a cold hypotonic buffer composed of 10 mM MOPS at pH 7.2, 100 mM sucrose, 1 mM EGTA, and 2 mM PMSF, and the mixture was left on ice for 6 min. The cell suspension was homogenized using a Dounce glass homogenizer. A cold hypertonic buffer consisting of 1.25 M sucrose and 10 mM MOPS at pH 7.2 was added to the cell homogenate in a ratio of 1.1 mL per gram of cells. The volume was then doubled by adding isotonic buffer, which included 2 mM PMSF and 2 mg/mL BSA. The homogenate was centrifuged at 1,000 x g for 10 min at 4°C, and the supernatant was collected. This step was repeated twice. Mitochondria were isolated by centrifuging the supernatant at 11,000 xg for 10 min at 4°C and washed once with isotonic buffer, excluding BSA. Finally, the pellet was resuspended in isotonic buffer, and the protein concentration of the isolated mitochondria was measured using the Bradford assay. HeLa and HEK293T-derived mitochondria required for immunoprecipitation (for western blot, mass spectrometry, and nanoString analyses) were isolated using a teflon-glass homogenizer as previously described.[85] Briefly, the cell pellet was resuspended in THE buffer (10 mM HEPES/KOH, 300 m Trehalose, 10 mM KCl, 1 mM EGTA, pH 7.4) supplemented with 1% BSA and 1mM PMSF, and incubate for 10 min or 15min on ice, for HEK293T or HeLa cells, respectively. The suspension was homogenized by 20 (HEK293T) or 30 (HeLa) strokes at 800 rpm. Cell debris and unbroken cells were removed by centrifugation, first, at 400 xg, 10min, 4°C, and then at 800 xg, 10min, 4°C. Mitochondria were sedimented at 11,000 xg, 10min, 4°C. After discarding the supernatant, the mitochondrial pellet was washed by resuspension in THE buffer, and the protein concentration of isolated mitochondria was determined using the Bradford assay.

Mitochondria swelling and protease-protection assay

Mitochondrial swelling experiments were performed as previously described.[86] Briefly, intact mitochondria were resuspended in either SEM buffer (250mM sucrose, 1mM EDTA, and 10mM MOPS pH 7.2), or the hypotonic EM buffer (1mM EDTA, and 10mM MOPS pH 7.2) to permeabilize the outer membrane. Proteinase K (PK) was added and samples were incubated on ice for 10min.To

access matrix proteins, mitochondria resuspended in EM buffer, were sonicated for 3 × 30s in the presence of (PK). Proteolytic activity was stopped by addition of 2mM phenylmethylsulphonyl fluoride (PMSF) and further 10-min incubation on ice. The samples were loaded on 10%–18% Tris-Tricine gradient gels under denaturing conditions and analyzed by western blotting.

Radioactive labeling of mitochondrial translation products

Mitochondrial translation products were labeled with radioactive [^{35}S]-methionine as previously described with minor modifications.[87] Briefly, cells were incubated with methionine-free DMEM medium at 37°C for 10 min. Next, cells were incubated with methionine-free DMEM containing emetine (100 μg/mL, Merck) for 10 min, then 200 μCi/mL [35S]-methionine was added to the medium and cells were incubated at 37°C for 1 h. After the incubation, cells were recovered, and equal amounts were loaded on a 10–18% Tris-Tricine gradient gel. The proteins were transferred to PVDF membranes and exposed to Phosphor Screens for digital radiography. The radioactive signal was detected on a Typhoon scanner (GE Healthcare). Quantification of the autoradiography images in Figures 3 and 6 was performed using FIJI software as follows: First, a manual threshold was determined to separate the background from the regions of interest. The values of background pixels were set to zero. Then, for the individual band or the total lane, the sum of the values over the threshold (integrated density) was obtained.

Cellular fractionation

For the fractionation of HeLa cells, the cell suspension was homogenized as described before in the Isolation of Mitochondria section, except for the absence of BSA in the Isotonic buffer. After homogenization and sedimentation of the cell debris and unbroken cells, the protein concentration of the suspension (post-nuclear supernatant, PNS) was determined using the Bradford assay. The suspension was diluted to 1 mg/ml concentration and 500 μL was centrifuged in the ultracentrifuge at 100,000 xg for 60 min at 4°C. The supernatant was collected in a fresh tube representing a cytosolic fraction. The pellet was resuspended in the isotonic buffer (equal volume to the initial fraction) and represented as an organelle fraction. Equal volumes of initial (PNS), cytosolic (soluble), and organelle (pellet) fractions were analyzed by SDS-PAGE and immunodetection.

Steady-state analysis of protein level with western blotting

Proteins derived from either whole cells or isolated mitochondria were loaded and separated on NuPage Bis-Tris 4-10% SDS gels or 10–18% Tris-Tricine gradient gels and transferred to PVDF membranes. Western blotting was performed following standard procedures. Primary antibodies were incubated overnight and were as follows: ATP5B, TIM44, TIM10B (custom-made raised in rabbit); SDHA (Thermo, 459200); MRPL1 (Proteintech, 16254-1-AP); MRPL53 (Proteintech, 16142-1-AP); MRPS25 (Proteintech, 67903-1-Ig); b-tubulin (abcam, AB6046), bS16m (Proteintech, 16735-1-AP); uS7m (Proteintech, 26828-1-AP); mL37 (Proteintech, 15190-1-AP); HSP90 (Cell Signaling, 4874S); FN3K (Proteintech, 14293-1-AP); FLAG (Sigma-Aldrich, F1804); TOM20 (Proteintech, 11802-1-AP). Secondary antibodies were goat anti-Rabbit and anti-mouse conjugated to horse-raddish peroxidase (Dianova).

RNA extraction, cDNA synthesis and qRT-PCR

RNA was extracted from cells using RNA Clean&Concentrator kit (Zymo Reseach, R1091) according to the manufacturer's protocol with minor changes. Adequate amount of TRIzol (Invitrogen) was added to the cells and incubated for 5 min at 24°C. A volume of cloroform equal to one-fifth of the TRIzol volume was added to the cells, and they were subsequently vigorously vortexed for 15 s. After a 3-min incubation at 24°C, samples were centrifuged at 12000xg and 4°C for 15 min. The aqueous upper phase was separated and mixed with 1:1 volume of pure ethanol and loaded to the purification columns. From here, the manufacture's protocol was precisely followed and RNA was eluted in RNAse/DNase free water, measured with Nanodrop (Thermo) and stored at −80°C until use. cDNA was synthesized from 1 μg of RNA, using the First Strand cDNA Synthesis kit (Thermo Scientific, K1612) and random hexamer primers. The qRT-PCR was performed using the SensiMixTM SYBR Low-Rox Obe Step kit (Bioline, QT625-02), in a QuantStudio 6 flex cycler (Applied Biosystems). The sequence of the primers is available upon request.

DNA extraction, mtDNA copy number measurement

Genomic DNA was extracted from cells using PureLink Genomic DNA mini kit (K182001, Thermo Fisher) according to the manufacturer's protocol and the eluted DNA was used to quantify the mtDNA copy number. TaqMan Universal PCR master mix (4326708, Applied Biosystems) and TaqMan pre-designed gene expression assay primers were utilized to quantify 3 mitochondrial-encoded genes (MT-RNR2, MT-AFP6, MT-ND2) and a nuclear one (18S rRNA) in a final volume of 8 μL. The reaction program included a 2 min hold at 50°C followed by a 10 min hold at 95°C, and 40 cycles of 15 s at 95°C and 1 min at 60°C.

FLAG immunoisolation

Protein complex isolation using FLAG immunoisolation was carried out following previously published methods. First, one milligram of isolated mitochondria was solubilized at a protein concentration of 1 mg/mL in lysis buffer (50 mM Tris/HCl pH 7.4, 150 mM NaCl, 10% glycerol, 10 mM $MgCl_2$, 1% Digitonin, 1 mM PMSF, 1x complete protease inhibitor cocktail, and 0.08 U/μL RiboLock RNase inhibitor) for 30 min on ice with intermittent mixing. The insoluble material was then removed by centrifugation at 10,000 xg for 10 min at 4°C. Subsequently, the lysate was mixed with anti-FLAG M2 Affinity Gel (Sigma-Aldrich) and incubated for 1 h at 4°C. The unbound fraction was removed, and the resin was washed with washing buffer (50 mM Tris/HCl pH 7.4, 150 mM NaCl, 10%

glycerol, 10 mM $MgCl_2$, 0.1% Digitonin, 1 mM PMSF, 1x complete protease inhibitor cocktail, and 0.08 U/μL RiboLock RNase inhibitor). The protein complexes were then eluted with 0.4 mg/mL FLAG peptide in washing buffer for 30 min at 4°C. Equal quantities of material were subjected to analysis by SDS-PAGE and western blotting. For RNA isolation and nanoString analysis, the input and eluate samples were mixed with 1 mL Trizol reagent (Thermo Fisher) and processed as described below.

Analysis of mitochondrial RNA abundance by nanoString

The input and eluate fractions from the immunoisolation were mixed with Trizol reagent (Thermo Fisher), and the RNA was purified using the RNA Clean & Concentrator kit (Zymo Research) according to the manufacturer's instructions. Equivalent amounts of RNA were mixed with a TagSet-24 and detection primers (IDT) previously used to detect mitochondrial transcripts.[58] Next, the samples were processed and analyzed in a nCounter MAX analysis system (nanoString) following the manufacturer's instructions. The acquired data were analyzed with nSolver software (nanoString).

Sample preparation for LC-MS

Immunoisolated protein samples were precipitated overnight at −20°C with five volumes 100% ice-cold acetone. Precipitated proteins were pelleted for 30 min at 13.000 g, the pellet washed with 80% (v/v) ice-cold ethanol, centrifuged as above, and dried at room temperature for 3–4 min. Dried proteins were re-dissolved in 1% (w/v) RapiGest (Waters) in 25 mM ammonium bicarbonate buffer (ABC) and sonicated in a BioRuptor device (Diagenode) with 30s on-and-off cycles for 10 min before reduction with dithiothreitol (DTT) and alkylation with 2-iodoacetamide (IAA). Protein digestion was performed in 25 mM ABC at 37°C with trypsin (Promega) at an enzyme-to-protein ratio of 1:20 (w/w) over night. The digestion was stopped by adding trifluoroacetic acid (TFA) to a final concentration of 1% (v/v). After centrifugation of hydrolyzed and precipitated RapiGest peptides in the supernatant were dried by vacuum centrifugation.

LC-MS/MS acquisition

Peptide samples were analyzed by data-independent acquisition (DIA) mass spectrometry using a timsTOF Pro2 (Bruker) mass spectrometer coupled to an Ultimate 3,000 RSLCnano UHPLC system (Thermo Fisher Scientific) in injection triplicates. Dried peptides were re-dissolved in 2% (v/v) acetonitrile (ACN), 0.05% (v/v) TFA in water and injected into the UHPLC system, where they were concentrated on a C18 PepMap100-trapping column (0.3 × 5 mm, 5 μm; Thermo Fisher Scientific) and separated on an analytical C18 column (Column Aurora with CSI, 25cm x 75umx1.6um, IonOpticks) using a 105 min linear gradient of 10–46% buffer B (80% (v/v) ACN/0.1% (v/v) formic acid (FA) in water) at 200 nL/min. MS data of eluting peptides were acquired using a standard DIA-PASEF method for long gradients with 32 constant-size isolation windows across the 400-1,200 m/z range, a mobility range of 0.6–1.43 and 1.8 s cycle time in a high sensitivity detection mode.

LC-MS/MS data analysis

Spectronaut (Biognosys; version 18.3) directDIA analysis of the generated MS/MS data was performed with default settings. Spectra were searched against a spectral library generated by Spectronaut from the UniProtKB human reference proteome (release 2022-10-12; 20,607 entries) for protein identification. A differential abundance analysis with normalized signal intensities was performed, comparing samples of the recombinant group (FN3K-FLAG) with the control (three biological replicates in the form of three technical replicates for each group), returning log transformed abundance ratios (fold changes) for the identified proteins. Proteins with a q-value of $\leq$0.01 and an average fold change of $\geq$0.5 (or $\leq$ - 0.5 for negative abundance ratios) were considered statistically to be enriched or depleted in the recombinant group.

Table S3 contains all enriched and depleted proteins after FN3K-FLAG immunoisolation as identified by Spectronaut.

QUANTIFICATION AND STATISTICAL ANALYSIS

Statistical analysis was performed using Graphpad Prism v 9.0. Statistical details, regarding type of tests used, *n* values and *p*-values are indicated in the corresponding figure legend for each experiment. In general, n represents either number of cells or number of biological replicates. Data are represented as average with SEM. Significance is determined by *p* values <0.05.